2009

Multiple – Wavelength Catalogs of the Point Sources in the South Ecliptic Pole Region Detected by Blast

Jens von der Linden
University of Pennsylvania, jensvonderlinden@gmail.com

Multiple – Wavelength Catalogs of the Point Sources in the South Ecliptic Pole Region Detected by Blast

Abstract
The goal of this project is to examine the far - infrared sources in the South Ecliptic Pole region (SEP) observed by the Balloon-Borne Large Aperture Submillimeter Telescope (BLAST). A primary science goal is to understand star formation processes. Most of the sources are assumed to be luminous infrared galaxies (LIRGs), in which high rates of star formation are believed to be occurring. The BLAST experiment mapped the 10 SEP at three wavelengths (250, 350 and 500 μm). To aid future studies of the SEP, three lists of interesting sources were created with an IDL source extraction algorithm. The first list is a catalog of all 5 σ sources and their counterparts. The second list contains sources which have unambiguous counterparts in the three wavelengths. The sources of the third list are likely to be high redshift. Spectral Energy Distributions (SED) were fit to each of the listed sources with an IDL SED fitter. Using the SED, preliminary estimates of luminosity and star formation rates can be made. The combined and unambiguous catalogs can be used to select targets for future observations. The third list will be especially useful for selecting high redshift LIRGs for future observations. Many of the presumed high redshift sources are unrealistically bright. It is possible that they are high redshift sources which are gravitationally lensed and magnified by clusters. The number of bright high redshift sources identified was used to test a recent theoretical model of the abundance of clusters.

Keywords
BLAST, CIB, Cosmic Infrared Background, star formation, South Ecliptic Pole, SEP, Natural Sciences, Physics and Astronomy, Mark Devlin, Devlin, Mark

Disciplines
Astrophysics and Astronomy | Cosmology, Relativity, and Gravity | Physical Sciences and Mathematics | Physics

Multiple – Wavelength Catalogs of the Point Sources in the South Ecliptic Pole Region Detected by Blast

Thesis

Jens von der Linden

05/08/2009

Table of Contents

Abstract

The goal of this project is to examine the far - infrared sources in the South Ecliptic Pole region (SEP) observed by the Balloon-Borne Large Aperture Submillimeter Telescope (BLAST). A primary science goal is to understand star formation processes. Most of the sources are assumed to be luminous infrared galaxies (LIRGs), in which high rates of star formation are believed to be occurring. The BLAST experiment mapped the 10 deg^2 SEP at three wavelengths (250, 350 and 500 μm). To aid future studies of the SEP, three lists of interesting sources were created with an IDL source extraction algorithm. The first list is a catalog of all 5 σ sources and their counterparts. The second list contains sources which have unambiguous counterparts in the three wavelengths. The sources of the third list are likely to be high redshift. Spectral Energy Distributions (SED) were fit to each of the listed sources with an IDL SED fitter. Using the SED, preliminary estimates of luminosity and star formation rates can be made. The combined and unambiguous catalogs can be used to select targets for future observations. The third list will be especially useful for selecting high redshift LIRGs for future observations. Many of the presumed high redshift sources are unrealistically bright. It is possible that they are high redshift sources which are gravitationally lensed and magnified by clusters. The number of bright high redshift sources identified was used to test a recent theoretical model of the abundance of clusters. This technique could potentially be applied to other studies to constrain the abundance model.

Section 1: Introduction

Cosmologists are trying to explain how the stars of the universe have formed. Stars are formed when dense clouds of molecular gas collapse into plasma. When a large amount of gas is

contained in a small area many stars could be created in so called starbursts. Many starbursts are believed to be happening in dusty galaxies. These galaxies are called luminous infrared galaxies, as radiation from star formation processes is absorbed by dust and reemitted in the infrared. Although stars are still being formed in the universe there was a time of increased star formation in the early universe. The cosmic infrared background (CIB) is a trace of that period of star formation. Many experiments have been designed to deepen our understanding of star formation in the early universe. This project will analyze data from one such experiment, the Balloon-Borne Large Aperture Submillimeter Telescope (BLAST). BLAST measures the flux at three different wavelengths 250, 350 and 500. Flux is the energy of the electromagnetic radiation per unit time passing through a unit area.

This study made one step towards analyzing BLAST observations of the South Ecliptic Pole (SEP) region of space by cataloging infrared emitting sources to aid in selecting candidates for future observations. Sources were identified and cataloged with the help of IDL (Interactive Data Language) routines. The first catalog was a combined list of sources and their counterparts across the BLAST wavelengths. Counterparts are source identifications in similar positions in different wavelength maps that are believed to be the same source. In addition, catalogs of sources were created that can be well identified across the three wavelengths observed by BLAST and sources that appear to have a high redshift i.e. are very far away. Estimates of key parameters such as star formation rate, luminosity, temperature and redshift of the identified sources were added to the lists. The parameters were determined by fitting the flux measured across each of the BLAST wavelengths to a greybody distribution. The result is the spectral energy distribution (SED), the estimated flux across the whole spectrum of wavelengths. From the SED an estimate of temperature, redshift, luminosity and star formation rate can be made.

Some of the high redshift sources appeared to be very bright although they are far away. This may be explained by gravitational lenses. Gravitational lenses are massive objects that act similar to optical lenses in that they can magnify sources.

To place the experiment in a better context **section 2** will examine the significance of the cosmic infrared background (CIB) to understand the history of the star formation, as well as the history of infrared observations and where the BLAST experiment fits into the CIB research. In addition, cosmological terms such as redshift, SED and clusters will be explained. The IDL routines used to extract sources from BLAST maps, to categorize them into lists and to create SED fits, will be detailed in **section 3**. Finally, the properties of the sources in the SEP as well as the subsets of unambiguous and high redshift sources will be discussed in **section 4**. A conclusion on the probability of the bright high redshift sources being lensed will be drawn and their abundance will be compared to theoretical models.

Section 2: Background

CIB: A tracer of Star formation

The universe is believed to be about 13.7 billion years old. **Figure 1** summarizes the current understanding of the evolution of the universe. At the beginning is the Big Bang. The universe, originally confined to a point, expands. Inflation marks a period of exponential expansion. The Cosmic Microwave Background (CMB) provides evidence for both events. The CMB is the afterglow of the hot dense plasma which comprised the universe before expansion it was cooled by expansion and the first atoms formed. Atoms could no longer absorb the thermal radiation and this radiation has propagated to the local universe from the surface of last

scattering. Gravitational forces amplified inhomogeneities in the universe and led to the formation of structure. Gravitational forces dominated the evolution of early structures due to the dominance of weakly interacting dark matter. Finally a combination of gravitational, electromagnetic, and nuclear forces caused the formation of stars and galaxies.

BLAST and other infrared background experiments are designed to detect a tracer of early star formation, the Cosmic Microwave Background (CIB). As stars form, radiation is created by gravitational and nuclear processes. Much of this radiation is absorbed by dust surrounding star forming regions and reemitted at infrared wavelengths (Lagache et al. 2005). This extragalactic radiation of early star formation comprises the CIB. Although the infrared radiation originated from these star forming sources on large scales the CIB is isotropic (Hauser & Dwek 2001).

Three types of sources of the CIB are speculated to exist: luminous infrared galaxies (LIRGs), ultra luminsous infrared galaxies (ULIRGs) and hyper luminous infrared galaxies (HyLIRGs). LIRGs are galaxies with luminosities $L_{ir} > 10^{11} L_{\odot}$, ULIRGs have luminosities $L_{ir} > 10^{12} L_{\odot}$ and HyLIRGs have luminosities $L_{ir} > 10^{13} L_{\odot}$. The infrared sources are believed to have been created by mergers of gas rich spirals, which may result in star formation and star bursts (Sanders & Mirabel. 1996). Other phenomena such as active galactic nuclei which are believed to be accretion processes of large black holes also contribute to the CIB. Their contribution is estimated to be ~10% (Kashlinsky 2005) and thus marginal.

To be identified as CIB, it must be distinguished from other infrared radiation, mainly from the infrared foreground of the Milky Way and from the submm component of the cosmic microwave background.

CIB observation history

The CIB was first predicted by Partridge and Peebles (1967). It proved to be rather difficult to detect the CIB as its infrared signal is weak compared to foregrounds from our galaxy. For ground based observations, atmospheric emissions are a major cause of noise for CIB measurements. Galactic stars, zodiacal emission from dust in the Milky Way, the galactic cirrus and the infrared frequencies of the CMB all contribute to an infrared foreground that must be subtracted to improve the accuracy of CIB measurements (Kashlinsky. 2005).

Early infrared rocket and satellite studies of the CIB were inconclusive due to poorly developed detectors. The Infrared Astronomical Satellite (IRAS) was the first instrument to conduct an all sky infrared survey (Neugebauer et al. 1984). It mapped the sky at wavelengths of 12, 25, 60, and 100 μm. However, due to limited sensitivity and the inability to determine a zero point for brightness measurements, data analysis could at best indicate the evidence for the existence of the CIB (Boulanger & Perault. 1988). After subtraction of galactic infrared emissions a background was found in the 100 μm data. It was however uncertain if this was due to zodiacal light, false zero calibration or the CIB.

Two instruments on the Cosmic Background Explorer (COBE) satellite (Fixsen et al. 1994), the Diffuse Infrared Background Experiment (DIRBE) and the Far Infrared Absolute Spectrophotometer (FIRAS) were able to prove the existence of an infrared background. DIRBE mapped the sky at 10 wavelength bands ranging from 1.25 to 240 μm (Silverberg at al. 1993). There was a detection of an isotropic CIB at the wavelengths of 140 and 240 μm and upper limits were determined for all other wavelengths (Hauser et al. 1998). With an improved model of zodiacal light the CIB was constrained from 1 to 300 microns (Wright. 2004). FIRAS was designed to measure the CMB from 125 μm to millimeter wavelengths. At 200 μm a residual

background in excess of the CMB and foreground noises was found which was believed to be the CIB (Puget et al. 1996). More recent studies have used devices such as the Near Infrared Spectrometer (NIRS) on IRTS (Noda et al. 1994), the Infrared Space Observatory (ISO) (Elbaz et al. 1999), and Spitzer (Papovich et al. 2004) and have covered more wavebands with higher sensitivities. **Figure 2** provides a summary of the experiments and measurements. In May 2009, the satellite Herschel will be launched. It will conduct the first all sky survey of submm wavelengths (Harwitt. 2004). BLAST, as a submm balloon borne telescope has prepared the way for Herschel.

BLAST

The Balloon-Borne Large Aperture Submillimeter Telescope (BLAST) is a suborbital experiment, designed to survey broadband spectral windows at wavelengths of 250, 350 and 500 μm with a resolution of 30'', 42'' and 60'', respectively (Pascale at al. 2008). BLAST (shown in **Figure 3**) will be able to detect infrared sources in a redshift z =1-4 range. BLAST served as a test for the SPIRE instrument on the Herschel telescope, as it used detectors and filters similar to the ones SPIRE will use. The results from BLAST could also influence the selection of the SPIRE observations. The science goals of BLAST are to constrain the redshift distribution and star formation rates of luminous infrared galaxies by determining their spectral energy distributions with wavelengths measured by BLAST and shorter wavelengths measured by IRAS, ISO and Spitzer. In addition, the spatial clustering of the luminous infrared galaxies should be determined. One engineering and two science flights were conducted with BLAST. The engineering flight was launched from Fort Summer, New Mexico (2003) and lasted 24 hours. The first science flight was conducted from the Swedish Space Corporation base

ESRANGE near Kiruna, Sweden to Victoria Island in northern Canada in 2005. The second science flight was launched in 2006 from the Williams Field Long Duration Balloon facility near McMurdo Station in Antarctica and collected 250 hours of data. Unfortunately, the BLAST telescope was destroyed by being dragged over ground for a distance of 200km by the landing parachute which had failed to separate from the instrument. In the 2006 flight over Antarctica, BLAST surveyed, among other regions, a $10\,\mathrm{deg}^2$ region near the South Ecliptic Pole (SEP). This region was analyzed for this project.

As the goal of this study is to create lists of sources of interest for future studies, some supplementary data are needed to facilitate a preliminary evaluation of the sources. Knowledge of the approximate redshift, luminosity, temperature and star formation rate will aid researchers in selecting sources for further study. Such data can all be determined / estimated from the Spectral Energy Distribution (SED) of the source.

Redshift

Redshifts can be determined by spectroscopy and photometry. Spectroscopic redshifts are the shifts of spectral lines of elements in the sources. This method requires surveys over a large range of wavelengths but provides precise redshift values. Measuring such a large amount of wavelengths in surveys over large areas would be prohibitive and impossible for faint galaxies (Connolly et al. 1995). For wide range observations, as done by BLAST, redshifts are determined by photometry. To calculate a redshift the observed intensities of colors of a source are compared to a template of colors and known redshifts of other galaxies (Benitez 1998, Stabenau 2008). The method of maximum likelihood estimation will be used to identify the most probable redshift. This method requires measurements to be taken in a few frequencies only,

however, it has a high uncertainty caused by color redshift degeneracy; i.e. red slightly shifted and blue highly shifted galaxies can look alike when observed. To reduce uncertainty in the redshift detection / determination, the data from other surveys can be included if counterparts of the sources are known. As the purpose of this project is directed to provide a preliminary list of sources for future observations, redshifts will be determined by a more simple method. An estimate can be made by assuming the intrinsic temperature. As the SEP sources are expected to have a Gaussian temperature distribution around 30K for a large number of sources, the approximation of a 30K intrinsic temperature can be made. This technique can only give an estimate of the redshift distribution over a large population.

Spectral Energy Distribution

The SED is the flux over a range of wavelengths of a source. Samples of SEDs of astrophysical objects are shown in **figure 3**. The infrared component of the SEDs of CIB sources is a grey body distribution and can be fitted to the three fluxes measured at the BLAST wavelengths. In some cases, however, BLAST had a source detection only in one or two bands. By using upper limits for the undetected bands, rough statements can be made. The so determined SED is not the intrinsic SED of the source but the apparent SED observed by the experiment due to the redshift of the source. The redshift must be known to calculate the intrinsic values. The redshift calculated in this way is based on the SED and an assumed temperature, so any intrinsic values calculated from the apparent ones and the redshift would be highly degenerate.

From the measured fluxes at the three wavelengths a SED can be fitted as a grey body distribution:

$$S_\nu = A\left(\frac{\upsilon}{\upsilon_0}\right)^{\beta} B_\upsilon(T) \quad (1)$$

where ν is the wavelength, T the Temperature and β the dust emissivity index set to 1.5.

Luminosity L is the power emitted by a source and is defined as the product of area A and flux F:

$$L = F \cdot A \quad (2)$$

A is the area of the surface of the sphere with a radius equal to the distance between source and observer.

$$L = F \cdot 4 \cdot \pi \cdot dL^2 \quad (3)$$

where dL is the luminosity distance.

The infrared luminosity L_{FIR} is defined according to Saunders et al. (1990) by integrating the flux from 80 to 1000 μm.

$$L_{FIR} = F_{80-1000\,\mu\mathrm{m}} \cdot 4 \cdot \pi \cdot dL^2 \quad (4)$$

In this context the redshift z is defined as:

$$z = \frac{T_{\mathrm{int}}}{T_{app}} - 1 \quad (5)$$

Where T_{int} is the intrinsic temperature and T_{app} the apparent temperature derived from the observed SED. To obtain a rough estimate of z, T_{int} can be assumed to be the average expected temperature of infrared sources: 30K.

According to Kennicutt et al. (1997) the star formation rate (SFR) of starbursts is strongly coupled to the far infrared luminosity. Young stars dominate the radiation and almost all their bolometric luminosity is absorbed and reemitted by dust in the infrared. An estimate of the SFR is:

$$SFR = \frac{L_{FIR}}{5.8 \cdot 10^{9} \cdot L_{\circ}} \cdot M_{\circ} yr^{-1} \tag{6}$$

where $L_{\circ}$ is the luminosity of the sun and $M_{\circ}$ is the mass of the sun.

However other factors such as gravitational lensing further complicate the determination of source properties.

Clusters & Gravitational Lensing

Gravitational lensing occurs when light from a distant source is bent around a massive object. This bending has an influence on the time it takes for the light to reach an observer and can magnify and can distort the apparent image of the source. The following discussion is based on Carroll (2004). **Figure 4** illustrates the angle relations between an observer and a gravitationally lensed image.

$$\vec{\beta} = \vec{\theta} - \frac{d_{LS}}{d_S} \hat{\alpha} \tag{7}$$

where the angles and lengths are shown in **Figure 4**.

Gravitational lenses cause a magnification of the flux of a source: more flux will be observed then is emitted by the source. This magnification μ is defined as:

$$\mu = |M| = \left| \frac{\partial \vec{\theta}}{\partial \vec{\beta}} \right| \tag{8}$$

where M is the magnification tensor. The magnification tensor can is determined by the distances and angles of the lensing map (**Figure 4**).

$$M = \left(\delta_{ij} - \frac{\partial \alpha^i}{\partial \theta^j} \right)^{-1} = \left(\delta_{ij} - \frac{\partial^2 \psi}{\partial \theta^i \partial \theta^j} \right)^{-1} \quad (9)$$

where the lensing potential ψ is defined as the integral of the geodesic paths Φ from the observer:

$$\psi(\vec{\theta}) = 2 \frac{d_{LS}}{d_L d_S} \int \Phi(d_L \vec{\theta}, s) ds \quad (10)$$

In the context of the BLAST maps gravitational lensing can make distant sources look close and cold through magnification. Gravitational lensing also indicates the presence of dark matter. The distribution of lensed sources can indicate the distribution of massive clusters even if these are not directly detected.

Section 3: Materials & Methods

The goal of this analysis is to create a combined source list for sources in the SEP and their counterparts across the three BLAST wave bands. These lists can be used for follow up observations and to estimate the distribution of gravitational lenses. To produce these lists, sources are first identified in all three individual wavelength flux maps of the SEP. An IDL source extraction algorithm applies a maximum likelihood method to find sources in each flux map. Next, a combined catalog of source counterparts in each of the three wavelengths is created. This combined catalog is searched for sources which fit criteria of the two proposed lists. For every source the SED is fitted and basic source properties, including an estimate of the redshift, are determined. Sources that are very bright at high redshifts are likely to be magnified by gravitational lenses. The following sections will describe the routines used to identify sources

and counterparts, the criteria used to create the unambiguous and high redshift lists as well as the SED fitter.

Source Extraction Algorithm

A BLAST map is shown in **Figure 5**. It is almost impossible to recognize sources except for a few very bright ones. A source extraction code is needed. We use an IDL algorithm that applies a maximum likelihood method to find sources in the maps. The following discussion of using the maximum likelihood function to find the signal to noise map is based on Serjeant et al. (2003), Downes et al. (1986), Arp et al. (1981) and a comment on Arp's statistics (Browne. 1982). The point spread function (psf) defines how a point source is displayed in the map. If a source is assumed to look like a flux f multiplied by the psf on a BLAST map, then the likelihood χ^2 of a source is defined as:

$$\chi^2 = \sum \frac{\left(y(x_0 - x) - f \cdot psf(x)\right)^2}{N(x_0 - x)^2} \tag{11}$$

where y is the value of the map and N the noise. Note that (11) is simplified to one dimension. To analyze the map a two dimensional equation must be used. To find the extrema of the likelihood, its derivative is set to zero:

$$\frac{d\chi^2}{df} = -2\sum \frac{y(x - x_0) - fpsf(x)}{N(x - x_0)} psf(x) = 0 \tag{12}$$

Solving for the flux and introducing Fourier transforms through the convolution theorem:

$$f = \frac{\sum y(x - x_0) \frac{1}{(N(x - x_0))^2} psf(x)}{\sum \frac{1}{(N(x - x_0))^2} (psf(x))^2} = \frac{\boldsymbol{F}^{-1}\left[F\left(y\frac{1}{N^2}\right)F(psf)\right]}{\boldsymbol{F}^{-1}\left[F\left(\frac{1}{N^2}\right)F\left(psf^2\right)\right]} \tag{13}$$

Propagating for errors the signal to noise ratio (S/N) of the flux is:

$$\frac{f}{\Delta f} = S/N = \frac{\boldsymbol{F}^{-1}\left[F\left(y\frac{1}{N^2}\right)F(psf)\right]}{\sqrt{\boldsymbol{F}^{-1}\left[F\left(\frac{1}{N^2}\right)F\left(psf^2\right)\right]}} \tag{14}$$

Fourier transforms can be efficiently calculated in IDL with the fast Fourier transform method. Positions of maxima in the S/N map are recorded by the IDL code in a catalog as sources along with their S/N as a multiple of the standard deviation. An S/N map is shown in **figure 6**.

Counterpart Search Algorithm

5 σ sources are significant enough to be included in a counterpart search. To find counterparts, an IDL algorithm is used to perform a search. For each 5 σ source the source catalogs at the other wavelengths are searched for counterparts which are within a search radius of the 5 σ sources. For the initial run the search radius of every source was $2.5 \cdot \Delta\alpha$, where $\Delta\alpha$ is the 1 - σ uncertainty in the position of the source. In addition, counterparts are required to have a signal to noise ratio of at least 3. According to Ivision et al. (2007) the uncertainty in the position $\Delta\alpha$ of a source is:

$$\Delta\alpha = 0.91 * FWHM \cdot \frac{1}{\sqrt{(S/N_{app})^2 - 2\beta + 4}} \tag{15}$$

where FWHM is the full width at half maximum of the telescope beam and β is the slope of the number counts of this population of galaxies, set to 1.5 in agreement with the BLAST maps. The position error has a complex relationship with the signal to noise ratio because there is a Malmquist bias in the flux limited telescope data which leads to an overestimation of the signal to noise ratio. BLAST can only detect sources down to a minimum flux and there are many more faint sources in the universe than bright sources. Uncertainty in the flux can lead to higher or

lower measured flux values, however, fluctuations below the BLAST sensitivity go undetected. Since there are more faint sources the probability for a detected source to have higher measured flux than intrinsic flux is greater than for a source to have a lower measured flux than intrinsic flux. This systematic overestimation of flux is the Malmquist bias. It is corrected in S/N:

$$S/N = \sqrt{(S/N_{app})^2 - (2\beta + 4)} \tag{16}$$

It is possible that two sources at different wavelengths are not physically related but simply are very close to each other (Browne & Cohen 1977, Downes et al. 1986). The probability of random association depends on the magnitude of the source, as fainter sources (large magnitude) will be denser and thus more likely to randomly be present in the search radius than bright sources (small magnitude). To quantify this probability one needs to calculate the expected number of randomly associated sources with the probability of random association P:

$$P \le P^* \tag{17}$$

where P^* is the probability of random association with a source that is of the same magnitude as the examined source. Assuming the probability of random association is P<<1, P is given by:

$$P = \pi r^2 N(m) \tag{18}$$

where r is the search radius and N the density of sources. BLAST has a lower limit on the flux it can detect so there is a maximum probability P_c for the highest magnitude source that can be observed. The expected number of randomly associated sources with (18) is then:

$$\text{for } P^* \ge P_c \qquad E = P_C \tag{19}$$

$$\text{for } P^* \le P_c \qquad E = P^* + \int \pi r^2 dN = P^* + \int \frac{P^*}{N(m)} dm = P^*\left(1 + \ln\frac{N_C}{N^*}\right) = P^*\left(1 + \ln\frac{P_C}{P^*}\right) \tag{20}$$

The Poisson probability can be calculated from the expected value:

$$P = e^{-E} \tag{21}$$

The maximum likelihood position of a source is calculated as the weighted average of the positions of its counterparts in the individual wavelength catalogs. The entry in the combined source catalog will register the position of the source, the S/N and the flux, noise and probability of random association of each of the counterparts. Having identified all counterparts the search for the unambiguous and high redshift sources can begin.

Unambiguous and High Redshift List Criteria

In regard to the source selection criteria, it is important to precisely define the terms 'source' and 'counterpart'. A counterpart is a source detection in one of the wavelength maps. A source is the collection of all counterparts located within the search radius. The unambiguous source list includes sources which have no confusion with their counterpart identification. They have no more than one counterpart per band. Sources are included in the unambiguous list if they

1) have a 5 sigma counterpart in one band and

2) have at most one 3 sigma counterpart within a 2.5 sigma search radius in each band

High redshift sources are likely to have an inverted SED as shown in **figure 8**. The high redshift catalog includes sources which

1) have a 5 sigma 500 μm counterpart,

2) have $S_{500} > S_{350} > S_{250}$ where S stands for the respective flux at each wavelength.

SED fitter

To make some preliminary estimates of temperature, redshift, luminosity and star formation rate of the sources, their spectral energy distributions (SED) must be determined. Before the SED is fitted, the flux values must be de-boosted to remove the Malmquist bias. To determine the bias in

the signal to noise ratios, it is necessary to create noise free simulated maps based on the source count model (Coppin et al. 2004). The distribution of the flux in the simulated maps is N(S_p). Assuming the flux $S_m \pm \sigma_m$ has been measured, the probability for true flux at some point of the BLAST map to be S_p given that the flux $S_m \pm \sigma_m$ was measured is:

$$P(S_p \mid S_m \pm \sigma_m, N(S_P)) = \frac{N(S_p)P(S_m \pm \sigma_m \mid S_p)}{P(S_m \pm \sigma_m)} \tag{22}$$

Assuming Gaussian noise the probability of the measured flux being $S_m \pm \sigma_m$ given that the true flux is S_p is:

$$P(S_m \pm \sigma_m \mid S_P) = A \cdot e^{\frac{(S_m - S_P)^2}{2\sigma_m^2}} \tag{23}$$

Then, the probability density function of the flux for the source of measured flux $S_m \pm \sigma_m$ is:

$$pdf = A \cdot e^{\frac{(S_m - S_P)^2}{2\sigma_m^2}} \cdot \mathrm{N}(\mathrm{S_p}) \tag{24}$$

As de-boosted flux the peak of the pdf is used i.e. the most likely flux.

The SED fitter is an IDL routine. Inputs are the flux and noise measured at each wavelength. If no counterpart is found, the flux on the map at the position of the combined source is used. For cases where the S/N at that position is above 2 σ, the flux on the map is taken as an upper limit. If the S/N is below 2 σ, the upper limit is set to the sum of the flux on the map and three times the noise at the position. The relative spectral response of each BLAST band is not exactly one wavelength but a range shown in **figure 9** (Pascale et al. 2008). To extract the flux at a single wavelength, the measured flux is put through a virtual bandpass. The SED is assumed to be a greybody, described by (1).

This distribution is fit to the inputs by minimizing χ^2 (Truch et al. 2008),

$$\chi^2 = (\tilde{S} - S) \cdot C^{-1} \cdot (\tilde{S} - S)^T \quad (25)$$

where S is the measured flux, and $\tilde{S}$ is the flux from the model, and C is the covariance matrix.

$$for \;\; i = j \;\; C_{ij} = \sqrt{\Delta_{n(i)}^2 + \Delta_{c(i)}^2} \quad (26)$$

$$for \;\; i \neq j \;\; C_{ij} = \sqrt{\Delta_{c(i)} \cdot \Delta_{c(j)} \cdot corr(i, j)} \quad (27)$$

where i and j are counters for the three wavelengths 250, 350 and 500 μm.

The diagonal elements are the quadrature sums of the noise Δ_n and the calibration error Δ_c at the respective wavelength. The off-diagonal elements are calculated by taking the square root of the product of the calibration errors of two bands and their correlation $corr(i, j)$.

To determine the error in the fit, a Monte Carlo simulation is used. The SED is refit 200 times with random noise added to the flux values to determine the uncertainty of the fit.

With the SED, the values of the apparent luminosity, star formation rate and redshift can be calculated using equations (4), (6) and (5). A typical SED fit is shown in **Figure 8**. A typical inverted SED fit from the high redshift catalog is shown in **Figure 9**.

Section 4: Major findings, results and analysis

In this section the basic properties of the source catalogs will be examined. These basic properties are the apparent temperature, redshift, luminosity and star formation rate distributions. The analysis will begin with the combined source catalog as it represents a population which was only selected to have a high S/N and should have similar properties to the whole source population observed by BLAST. The properties of the unambiguous and high redshift catalog

sources will be compared to the combined catalog sources and differences will be explained based on the selection effects of each catalog. Finally, uses for the catalogs will be proposed, based on the found properties. Source lists were made for 2 σ, 3 σ, and 5 σ sources of the 250, 350 and 500 BLAST maps. Combined source lists, high redshift source lists and unambiguous source lists were created with the criteria described in section 3. Table 1 shows the number of sources found for each list.

Table 1: Source Counts

Wavelength / S/N	250	350	500	combined	unambiguous	high redshift
2 sigma	6137	4515	3003			
3 sigma	2010	1302	1263	303	228	43
5 sigma	154	73	125			

Note: The S/N does not apply to combined, unambiguous and high redshift catalogs. See section 3 for the selection criteria.

A decrease in the number of sources observed is expected at larger wavelengths due to the decreased resolution of the telescope at these wavelengths.

Table 2 summarizes properties of the sources in the combined list. The average of the apparent temperature of the sources, 19 ± 15.4 K is within the range of the assumed average temperature of all sources 30K. A histogram of the apparent temperatures (**figure 10**) reveals a peak in number counts around 10K. This is not surprising as this corresponds to an SED with a peak at 250 microns, the wavelength at which BLAST is most sensitive. The average redshift 1.8 ± 2.69 is within the range most sources detected by BLAST are expected. With a histogram of the redshifts (**figure 11**) it can be seen that the number counts peak at redshifts close to 0. The few extremely high redshifts observed z >>10 are probably non real. Luminosities and the star

formation rates vary widely from dim to hyper-luminous galaxies as their standard deviation is more than one magnitude larger than their average values. As can be seen in the histogram plots (**figures 12 & 13**) of luminosity and star formation rate, two populations are observed. One population has luminosities around $10^8 L_\odot$ and star formation rates around $1 M_\odot$ and the other population has luminosities around $10^{13} L_\odot$ and star formation rates around $10^5 M_\odot$. Although it should be noted that for many luminosities and star formation rates the uncertainties are orders of magnitude. Keeping this in mind it is difficult to determine if the second population is composed of mainly LIRGs, ULIRGs or HyLIRGs. BLAST is designed to detect LIRGs so the detection of a large amount of low luminosity sources is surprising. The uncertainties of the low luminosity sources are rather high. If the luminosity histogram is redrawn including only sources with an uncertainty to luminosity ratio of less than 10 the population of low luminosity sources disappears (**figure 14**). It seems likely that the SED fits and corresponding properties of the supposedly low luminosity are ill determined because many of these sources only have one detection as can be seen from **table 2.**

Table 3 summarizes properties of unambiguous sources. The average values of the combined and unambiguous sources are similar. The average apparent temperature of the sources, 21 ± 16.9 K and the average redshift 1.8 ± 2.28 are both in the range of the averages of the combined source list. The redshift and temperature distributions are also similar as shown in **figures 15 & 16**. There are to be less extremely high redshift sources in the combined source catalog. This indicates that the unambiguous source catalog population is very similar to that of the combined source catalog population. But the unambiguous source list has less unrealistic extreme redshift sources. The luminosities and the star formation rates vary widely from dim to hyper-luminous galaxies as their standard deviation is more than one magnitude larger than their

average values. Again, the distributions of the luminosities and star formation rates (**figures 17 & 18**) are similar to the combined source list. Two populations are visible of sources with low luminosity and LIRGs. The low luminosity sources, however, have uncertainty to luminosity ratios greater than 10 as in the combined source list (**figure 19**).

A summary of the properties of the high redshift sources is shown in **table 4.** The average apparent temperature of the sources, 6.2 ± 2.28 K is low compared to the apparent temperature distribution of all sources. The temperature distribution (**figure 20**) has a cut off around 10K, due to the selection of inversed SEDs. The average redshift is high 4.9 ± 3.40 as is expected since the sources were selected to have a high redshift. This is also reflected in the redshift distribution (**figure 21**). There is a cut off in the luminosities and star formation rates around $10^{13} L_{\odot}$ and $10^{4} M_{\odot}$ (**figure 22 & 23**). Again, the uncertainties in these values are orders of magnitude. Most of the high redshift sources are at least LIRGs if not ULIRGs and HyLIRGs.

Many of the sources in the high redshift list seem to have surprisingly high luminosities for their expected redshifts as shown in **table 4**. Normally sources at high redshift should be faint as their emission should decay over large distances. The high luminosity could have three explanations:

1) The likely high redshift sources are in fact low redshift and relatively cold
2) The likely high redshift sources are high redshift HyLIRGs
3) The likely high redshift sources are high redshift gravitationally lensed sources.

Trentham (1995) and Broadhurst & Lehar (1995) referred to gravitational lensing to explain the brightness of a high redshift source in the IRAS survey. They estimated the likelihood of the source being lensed to be 0.25-0.3. In contrast to this study, they had the advantage of knowing the spectroscopic redshift of the source.

Lima et al. (2009) have done some recent work on estimating the abundance of gravitational lens clusters. However, the calculation did not confirm the number counts of likely lensed sources found in this study. Chapin et al. (2009) analyzed IRAS (low redshift due to limited sensitivity) sources and found no significant source population with temperatures below 23K. However, low temperatures are conditions for bright infrared sources. This indicates that low redshift galaxies are unlikely to be as bright as the sources in **table 4**. It seems likely that bright sources in the high redshift list are indeed high redshifts. An unknown portion of the sources could be intrinsically bright and the other portion could be magnified by gravitational lensing. If we could differentiate the two cases it would be interesting to compare the amount of lensed sources to theoretical models.

The combined and unambiguous source list can be used for future observations as catalogs of high S/N sources and their counterparts. The unambiguous source list may be more useful as it seems to include less unrealistic sources such as extremely high redshift sources. The high redshift source catalog may be used to select candidates for future high redshift observations. Also, it may constrain gravitational lensing models.

Section 5: Summary

For this study, maps from the Balloon-Borne Large Aperture Submillimeter Telescope (BLAST) experiment were analyzed. Combined, unambiguous and high redshift source lists with basic source properties were created to aid researchers in further studies of infrared objects in the SEP. The unambiguous source list may be especially useful as its sources have unique counterpart identifications and include fewer unrealistic extreme redshift sources. The high redshift catalog

will be useful for identifying high redshift LIRGs in the SEP for future observations. Many sources in the high redshift list were found to be very bright. It was concluded that they are either gravitationally lensed or hyper-luminous. If it can be determined which sources are lensed, it may be possible to test lens structure abundance models by comparing expected and measured lensed number counts.

Literature Cited

Arp H. 1981. The Astrophysical Journal. 250: 31-42.

Benitez N. 1998. arXiv:astro-ph/9811189v1

Broadhurst T, Lehar J. 1995. The Astrophysical Journal. 450: L41-L44.

Browne IWA. 1982 The Astrophysical Journal. 263: L7-L8.

Browne IWA & Cohen AM. 1977 Monthly Notices of the Royal Astronomical Society. 182: 181-187.

Boulanger F, Perault M. 1988. The Astrophysical Journal. 330: 964-985.

Carroll S. 2003. Spacetime & Geometry. Addison-Wesley.

Chapin EL, Hughes DH, Aretxaga I. 2009. Monthly Notices of the Royal Astronomical Society. 393: 653-662.

Connolly AJ, Csabai I, Szalay AS, Koo DC, Kron RG, Munn JA. 1995. arXiv:astro-ph/9508100v1

Coppin K, Halpern M, Scott D, Borys C, Chapman S. 2005. Monthly Notices of the Royal Astronomical Society. 357: 1022-1028.

Downes AJB, Peacock JA, Savage A & Carrie DR. 1986 Monthly Notices of the Royal Astronomical Society. 218: 31-62.

Elbaz D, Cesarsky CJ, Fadda D, Aussel H, Desert FX, Franceschini A, Flores H, Harwit M, Puget JL, Clements DL, Danese L, Koo DC, Mandolesi R. 1999. Astronomy & Astrophysics. 351: L37-L40.

Fixsen DJ, Cheng ES, Cottingham DA; Eplee RE, Jr., Isaacman RB, Mather JC, Meyer SS, Noerdlinger PD, Shafer RA, Weiss R, Wright E L, Bennett CL, Boggess NW, Kelsall T, Moseley SH, Silverberg RF, Smoot GF, Wilkinson DT. 1994. *Astrophysical Journal* **420**: 445–449.

Harwitt M. 2004. Advances in Space Research. 34: 568-572.

Hauser MG, Dwek E. 2001. Annual Review of Astronomy and Astrophysics. 39:249-307.

Hauser MG, Arendt Rg, Kelsall T, Dwek E, Odegard N, Weiland JL, Freudenreich HT, Reach WT, Silverberg RF, Moseley SH, Pei YC, Lubin P, Mather JC, Shafer RA, Smoot GF, Weiss R, Wilkinson DT, Wright EL. 1998. The Astrophysical Journal. 508: 25-43.

Ivison RJ, Greve TR, Dunlop JS, Peacock JA, Egami E, Smail I, Ibar E, van Kempen E, Aretxaga I, Babbedge T, Biggs AD, Blain AW, Chapman SC, Clements DL, Coppin K, Farrah D, Halpern M, Hughes DH, Jarvis MJ, Jenness T, Jones JR, Mortier AMJ, Oliver S, Papovich C, Perez-Gonzalez PG, Pope A, Rawlings S, Rieke GH,

Rowan-Robinson M, Savage RS, Scott D, Seigar M, Serjeant S, Simpson C, Stevens JA, Vaccari M, Wagg J, Willott CJ. 2007 Monthly Notices of the Royal Astronomical Society 380: 199-228.

Kennicutt RC. 1997. The Asophysical Journal. 498: 541-552.

Lagache G, Puget J-L, Dole H. 2005. Annual Review of Astronomy and Astrophysics. 43:727-768.

Lima M, Bhuvnesh J, Devlin M. 2009. submitted for publication in Monthly Notes of the Royal Astronomical Society.

Neugbauer G, Habing HJ, van Duinen R, Aumann HH, Baud B, Beichman CA, Beintema DA, Boggess N, Clegg PE, De Jong T, Emerson JP, Gautier TN, Gillett FC, Harris S, Hauser MG, Houck JR, Jennings RE, Low FJ, Marsden PL, Miley G, Olnon FM, Pottasch SR, Raimond E, Rowan-Robinson M, Soifer BT, Walker RG, Wesselius PR, Young E. 1984. The Astrophysical Journal. 278: L1-L6

Noda M, Matsumoto T, Matsuura S, Noguchi K, Tanaka M, Lim MA, Murakami H. 1994. The Astrophysical Journal. 428: 363-369.

Papovich C, Dole H, Egami E, Le Floc'h E, Perez-Gonzalez PG, Alonso-Herrero A, Bai L, Beichman CA, Blaylock M, Engelbracht CW, Gordon KD, Hines DC, Misselt KA, Morrison JE, Mould J, Muzerolle J, Neugebauer G, Richards PL, Rieke GH, Rieke MJ, Rigby JR, Su KYL, Young ET. 2004. The Astrophysical Journal Supplement Series. 154: 70-74.

Pascale E, Ade PAR, Bock JJ, Chapin EL, Chung J, Devlin MJ, Dicker S, Griffin M, Gunderson JO, Halpern M, Hargrave PC, Hughes DH, Klein J, MacTavish CJ, Marsden G, Martin PG, Martin TG, Mauskopf P, Netterfield CB, Olmi L, Patanchon G, Rex M, Scott D, Semisch C, Thomas N, Truch MDP, Tucker C, Tucker GS, Viero MP, Wiebe DV. 2008. The Astrophysical Journal. 681:400-414.

Patridge RB, Peebles PJE. 1967. The Astrophysical Journal. 147: 868-886.

Puget J-L, Abergel A, Bernard J-P, Boulanger F, Burton WB, Desert FX. 1996. Astronomy & Astrophysics. 208: L5-L8

Sanders DB, Mirabel IF. 1996. Annual Review of Astronomy and Astrophysics. 34: 749-92

Sauders W, Rowan-Robinson M, Lawrence A, Efstathiou G, Kaiser N, Ellis RS, Frenk CS. 1990. Monthly Notices of the Royal Astrophysical Society. 242: 318-337

Serjeant S, Dunlop JS, Mann RG, Rowan-Robinson M, Hughes D, Efstathiou A, Blain A, Fox M, Ivison RJ, Jenness T, Lawrence A, Longair M, Oliver S, Peacock JA. 2003 Monthly Notices of the Royal Astronomical Society. 344: 887-904.

Silverberg RF, Hauser MG, Boggess NW, Kelsall TJ, Moseley SH, Murdock TL. 1993. Proceedings of SPIE 180.

Stabenau HF, Connolly A, Bhuvnesh J. 2008. arXiv:0712.1594v2 [astro-ph]

Trentham N. 1995. Monthly Notices of the Royal Astronomical Society. 277: 616-626.

Truch MDP, Ade PAR, Bock JJ, Chapin EL, Devlin MJ, Dicker S, Griffin M, Gundersen JO, Halpern M, Hargrave PC, Hughes DH, Klein J, Mardsen G, Martin PG, Mauskopf P, Netterfield CB, Olmi L, Pascale E, Patanchon G, Rex M, Scott D, Semisch C, Tucker C, Tucker GS, Viero MP, Wiebe DV. 2008. The Astrophysical Journal. 681:415-427.

Wright EL. 2004. New Astronomy Reviews. 5-6:465-468

Acknowledgments

I would like to thank Prof. M. Devlin, for his time and patience as my advisor, as well as Dr. J. Klein, Dr. M. Lima**,** Dr. A. Mroczkowski, Dr. M. Rex, Dr. H. Staubenau, Mr. N. Thomas, Dr. M Truch, and the BLAST collaborators for their help and advice, and the College of Arts and Sciences and BLAST for travel funding to the Toronto BLAST collaboration meeting.

Figures

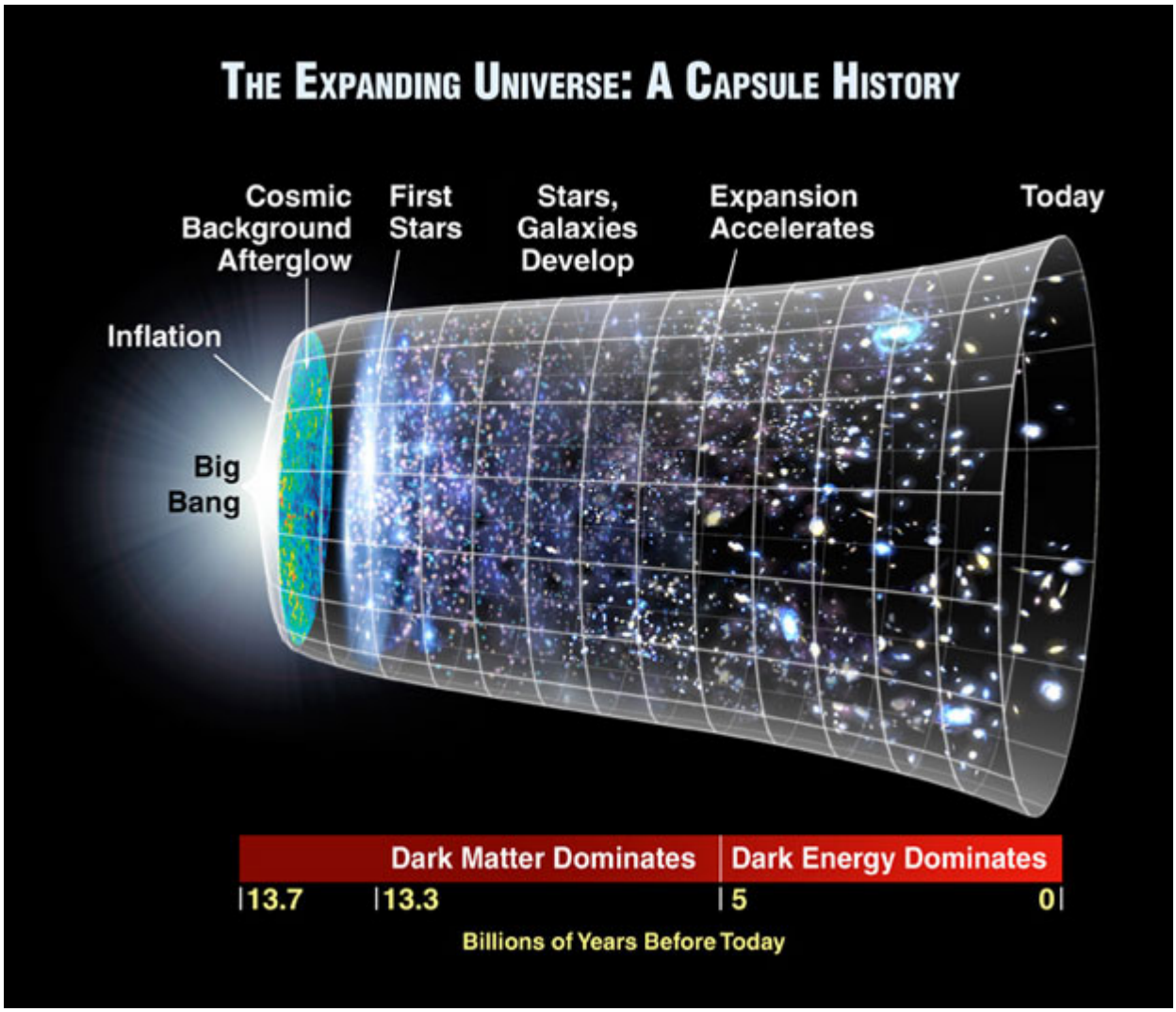

Figure 1: History of universe.

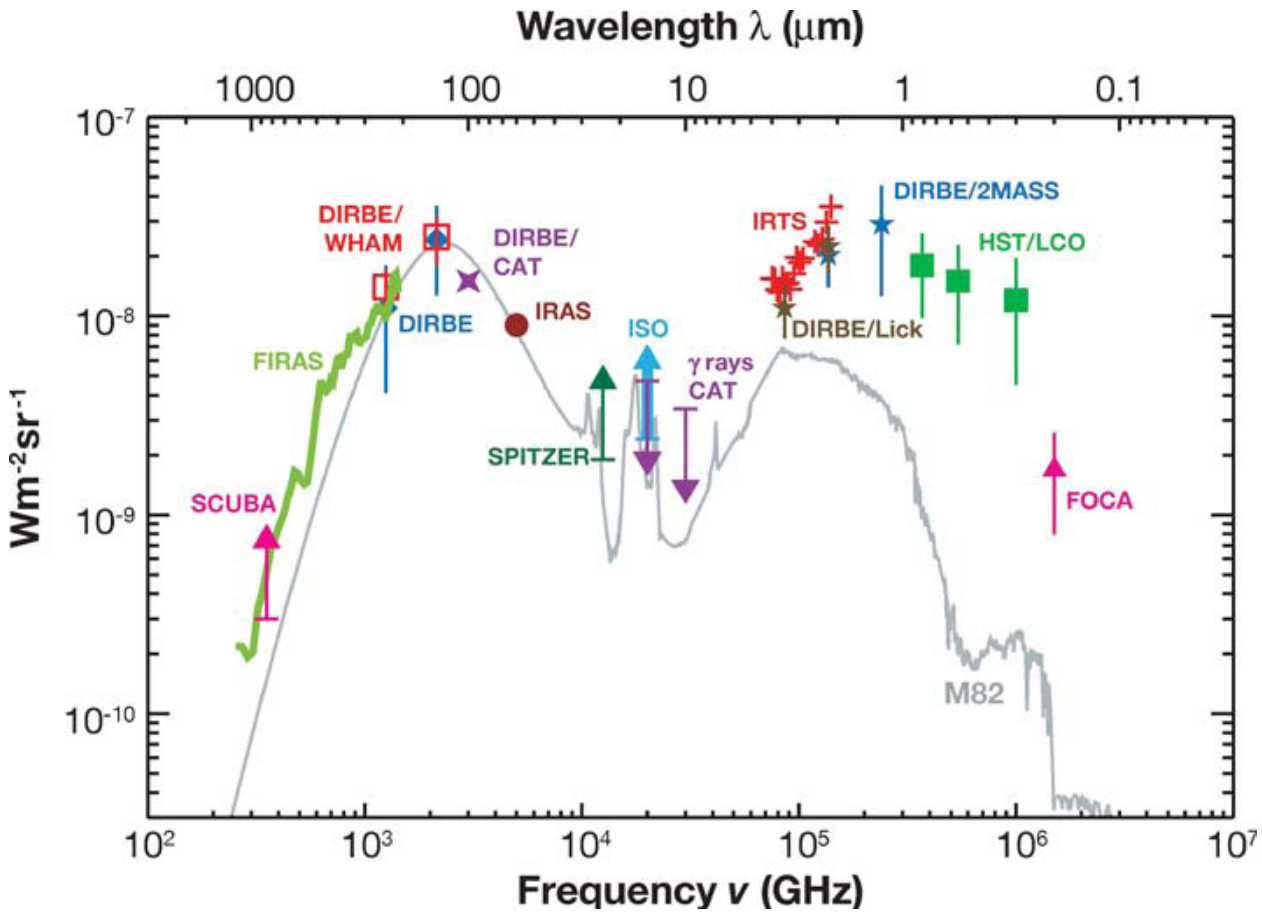

Figure 2: The extragalactic background over three decades in frequency from the near UV to millimeter wavelengths. Only strongly constraining measurements have been reported. (Lagache et al. 2005)

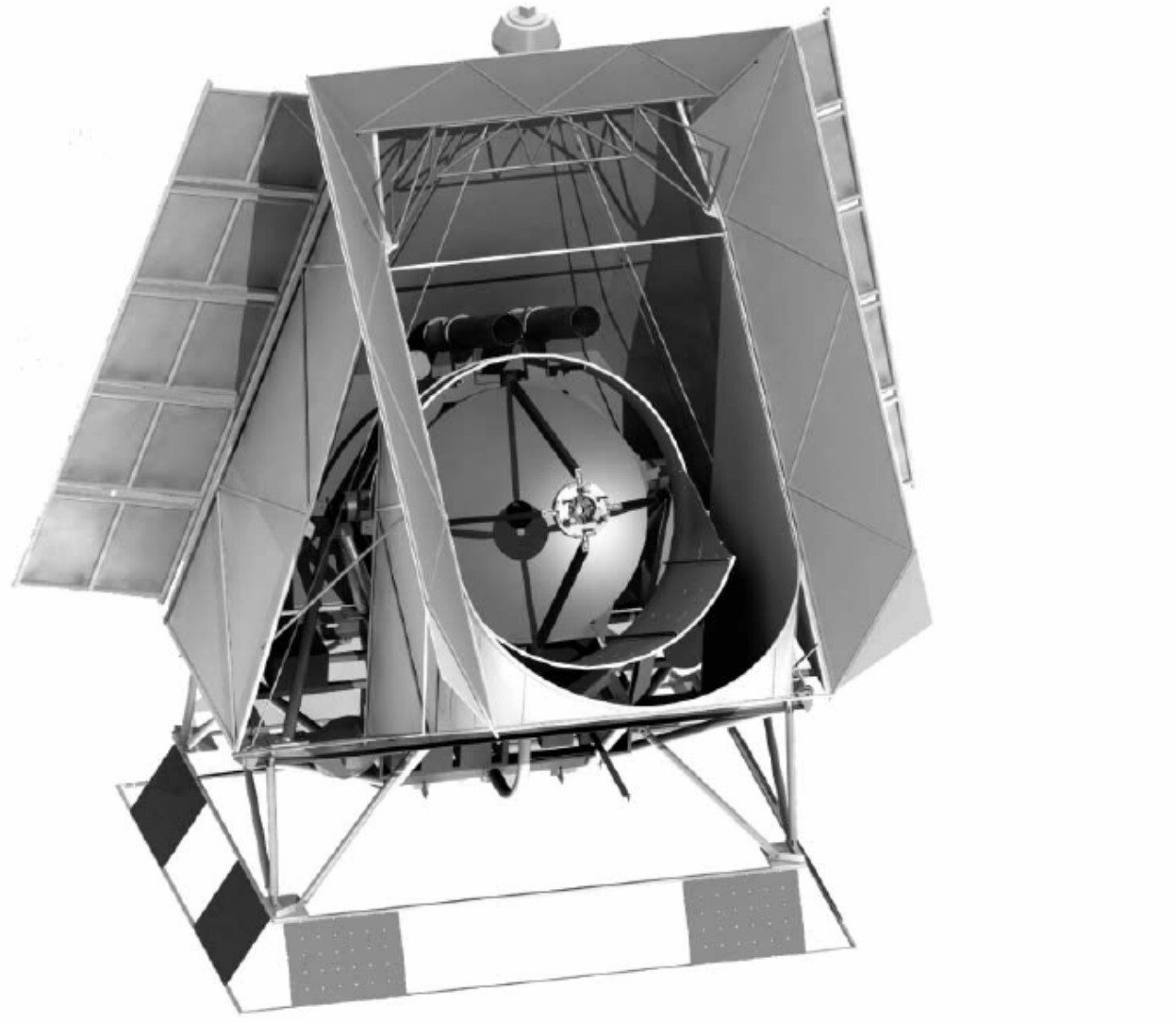

Figure 3: CAD image of the BLAST Gondola (Pascale et al. 2008)

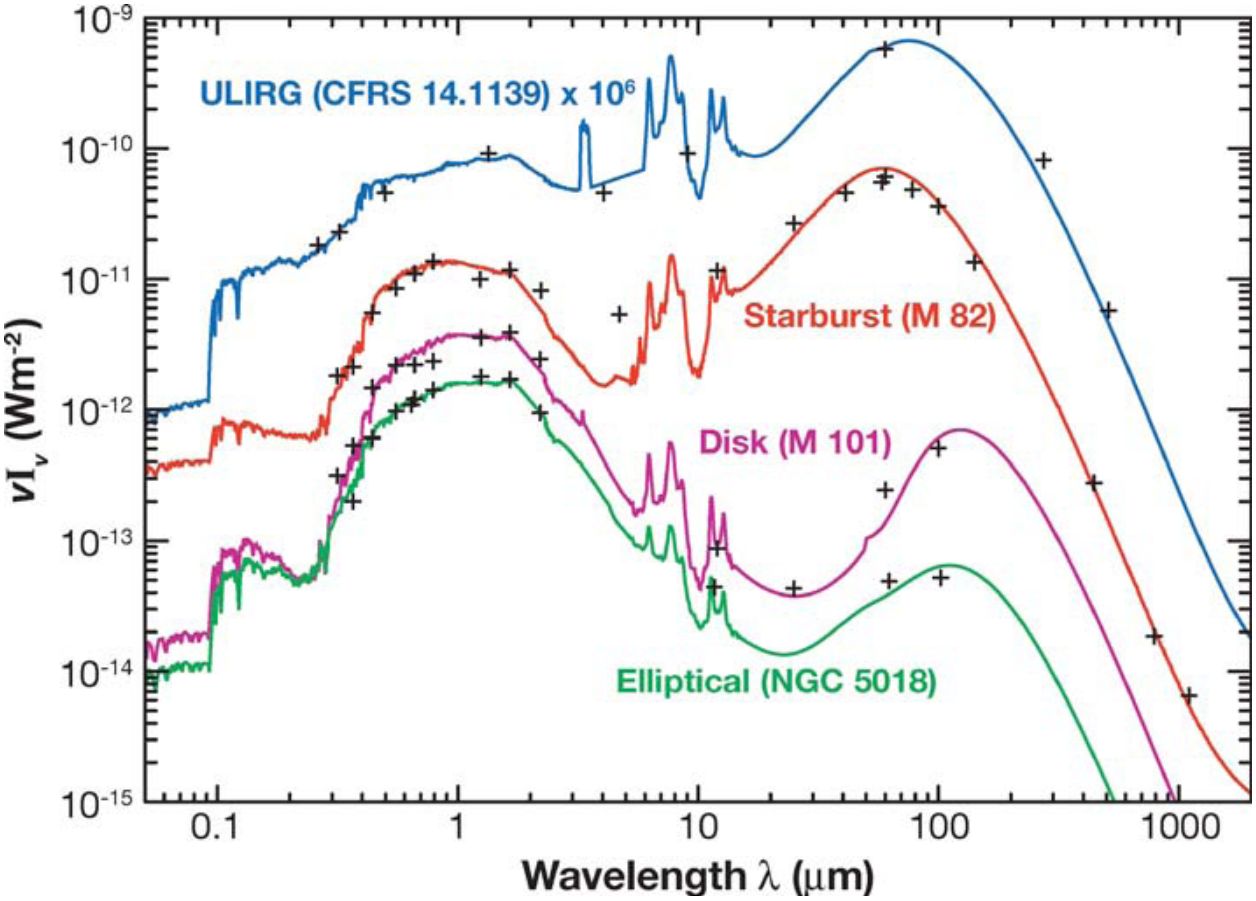

Figure 4: Spectral energy distributions of galaxies from the UV to the millimeter. The ULIRG is observed at redshift z = 0.66 and is represented here in the rest frame (from Galliano 2004) (Lagache et al. 2005)

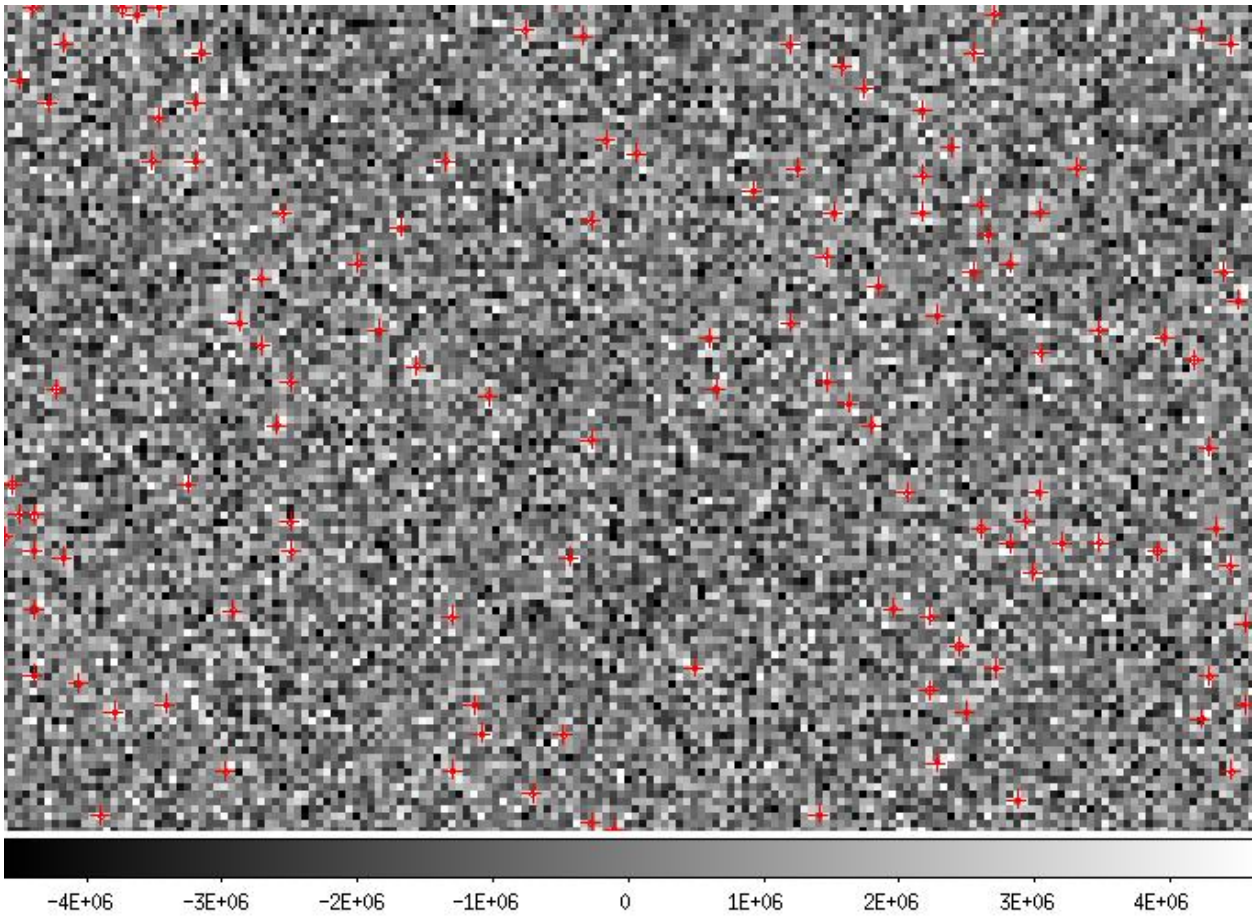

Figure 5: BLAST flux map. This is a ds9 screenshot. The red crosses mark positions of sources.

It is impossible to recognize sources from this image.

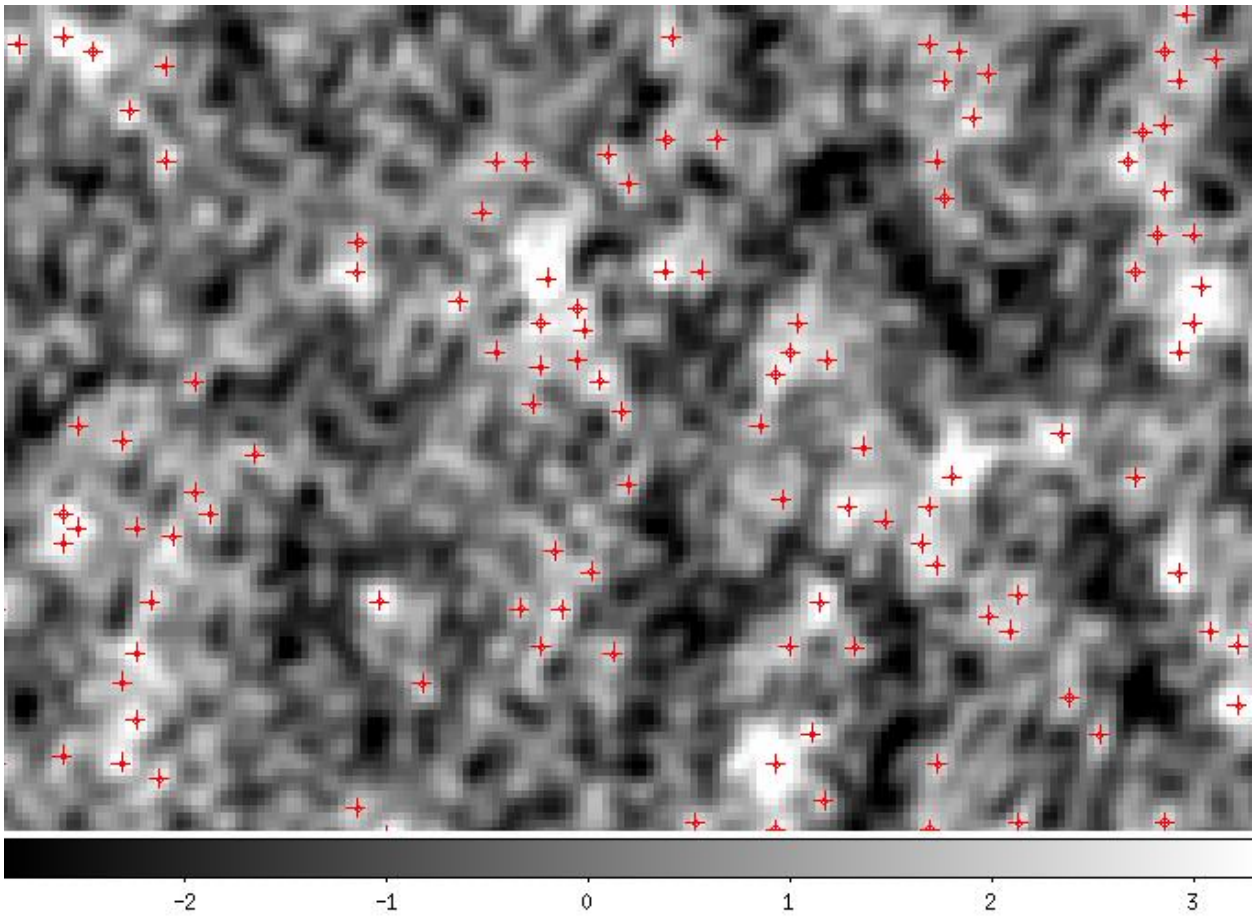

Figure 6: Signal to Noise map of the same region shown in Figure 3. Sources are maximas (red crosses) of the map and can almost be recognized with bare eye.

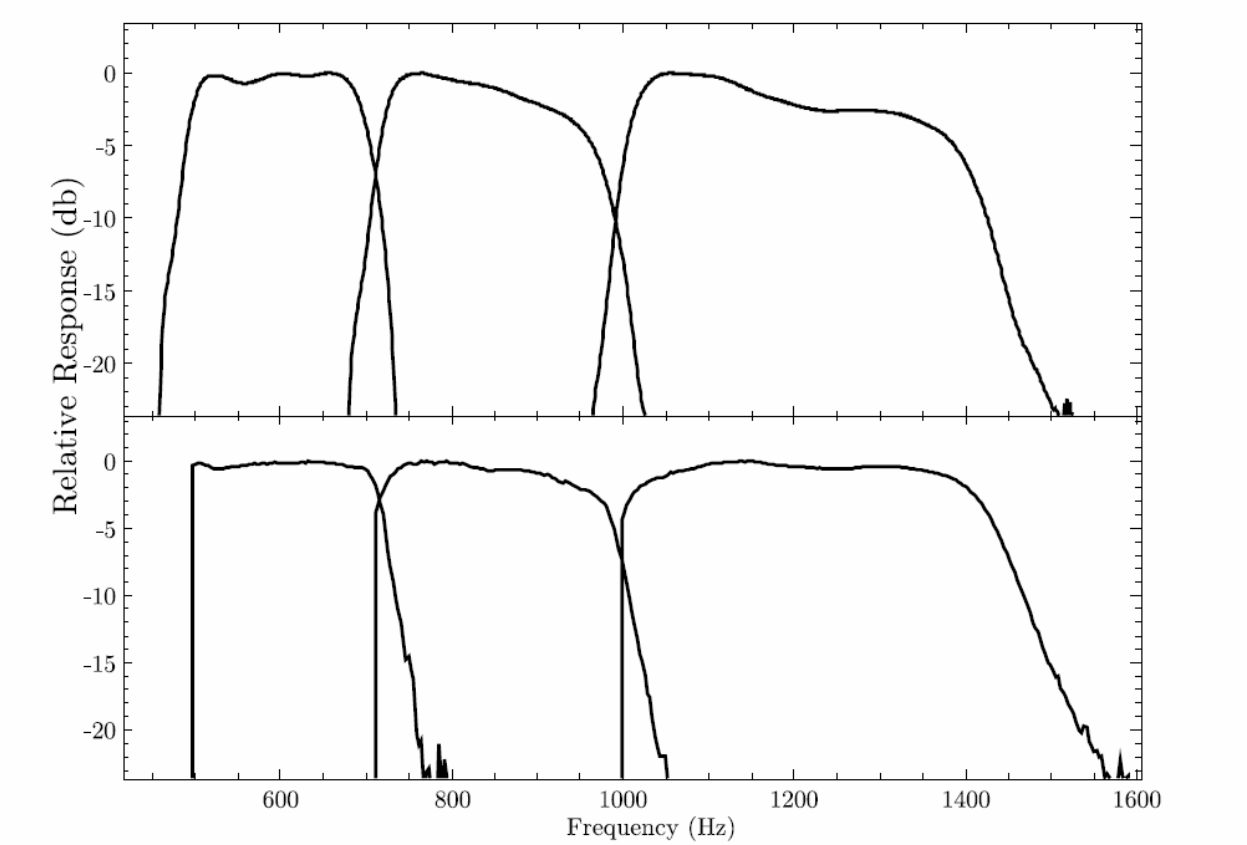

Figure 7: Relative Spectral response of the three BLAST bands. (Pascale et al. 2008)

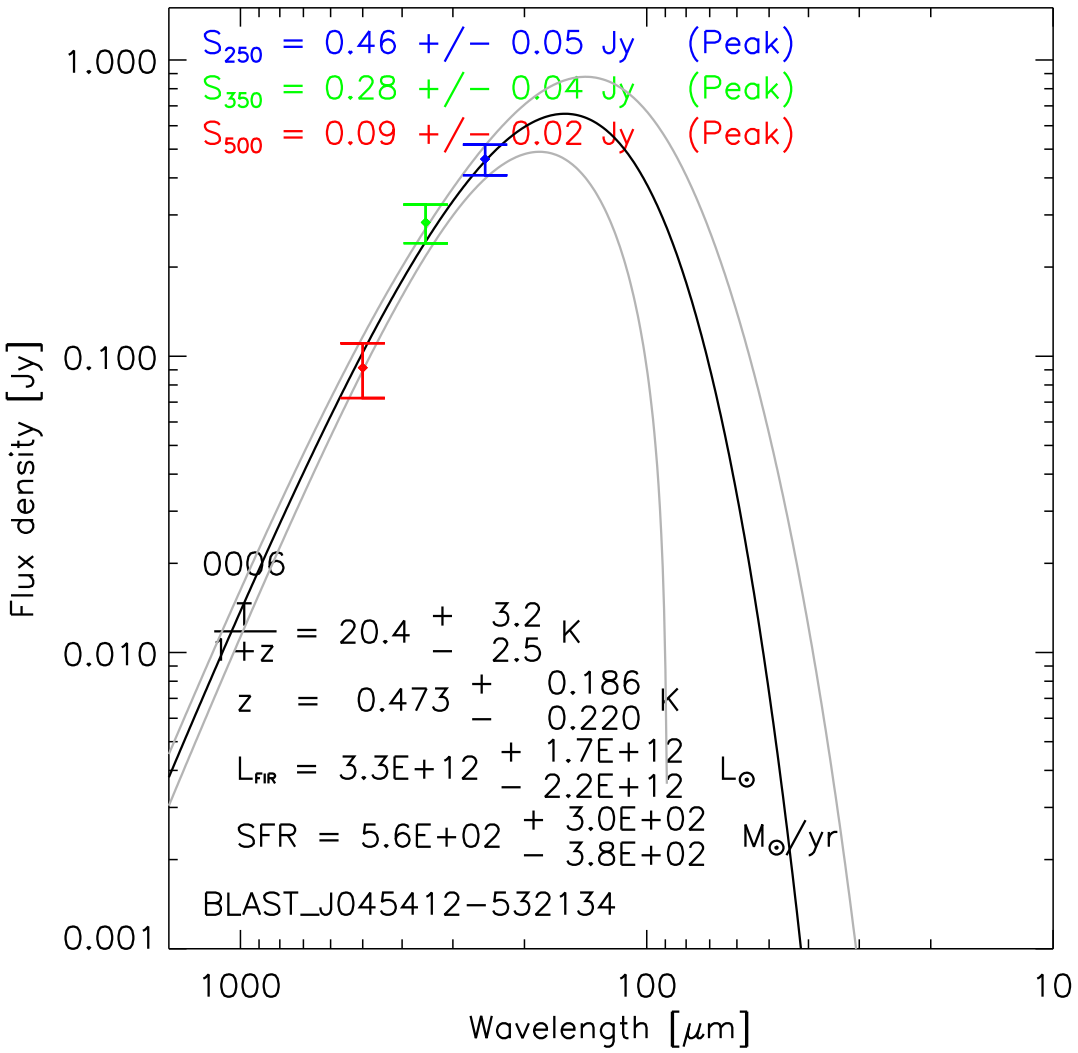

Figure 8: Typical SED fit. There are detections in all three wavebands.

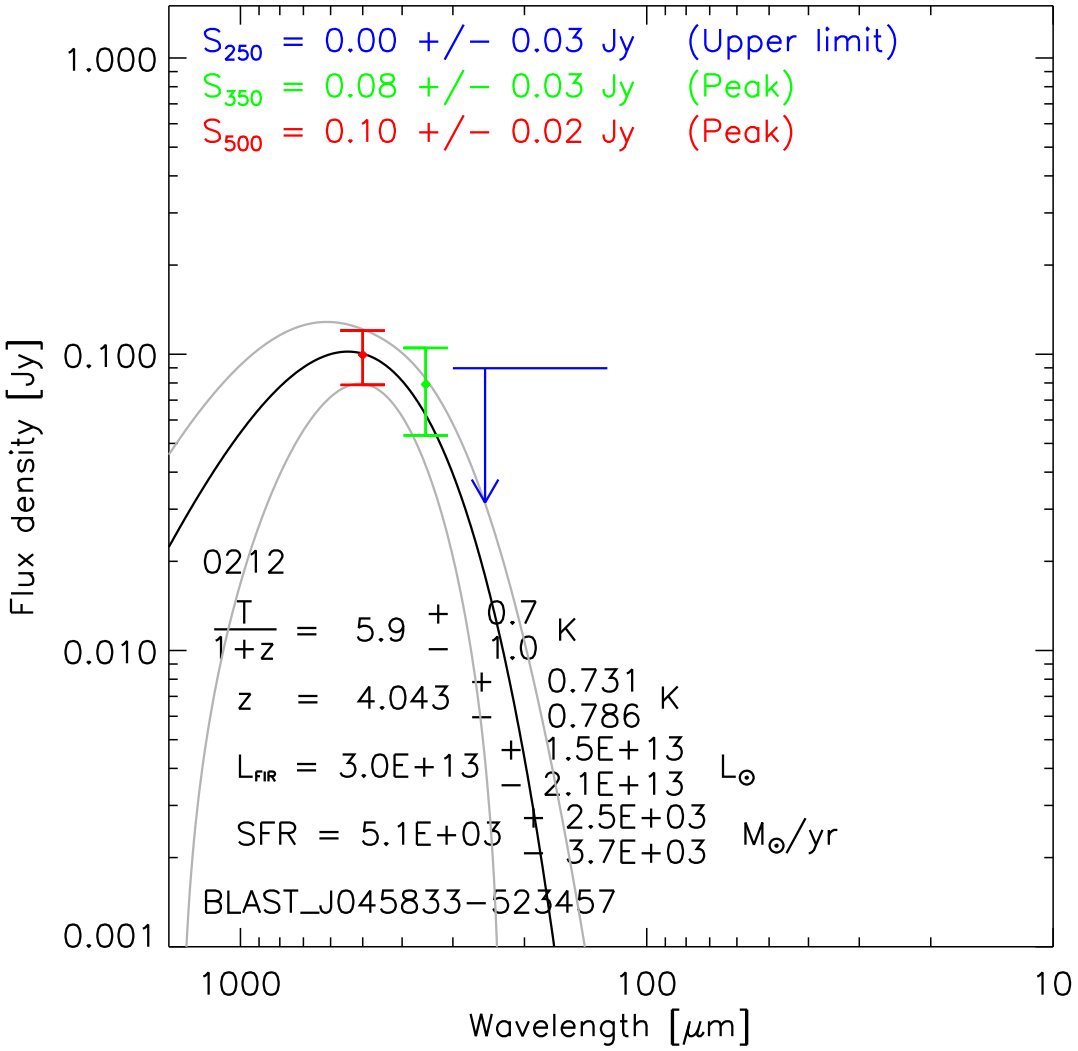

Figure 9: inverted SED fit. The 250 μm flux is an upper limit.

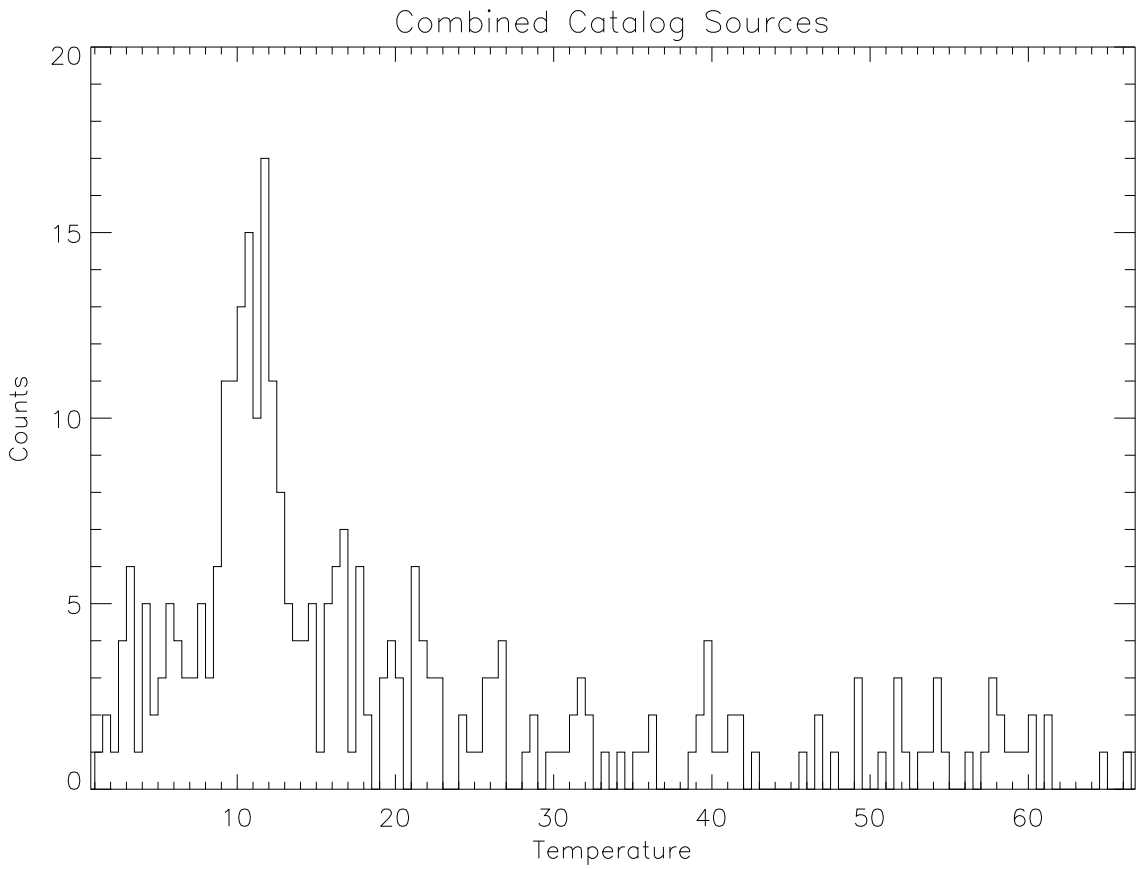

Figure 10: Apparent temperature histogram of the combined source list. Bin size is 0.2.

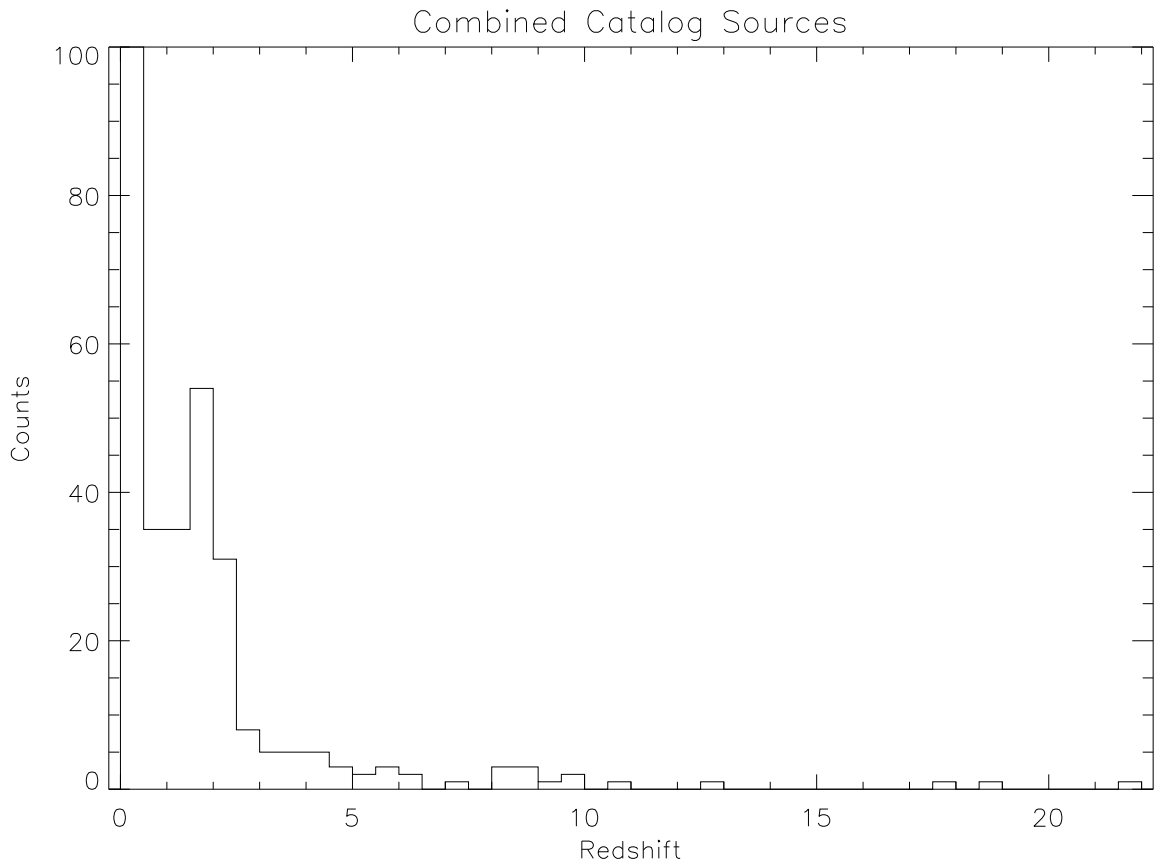

Figure 11: Redshift histogram of the combined source list. Bin size is 0.2.

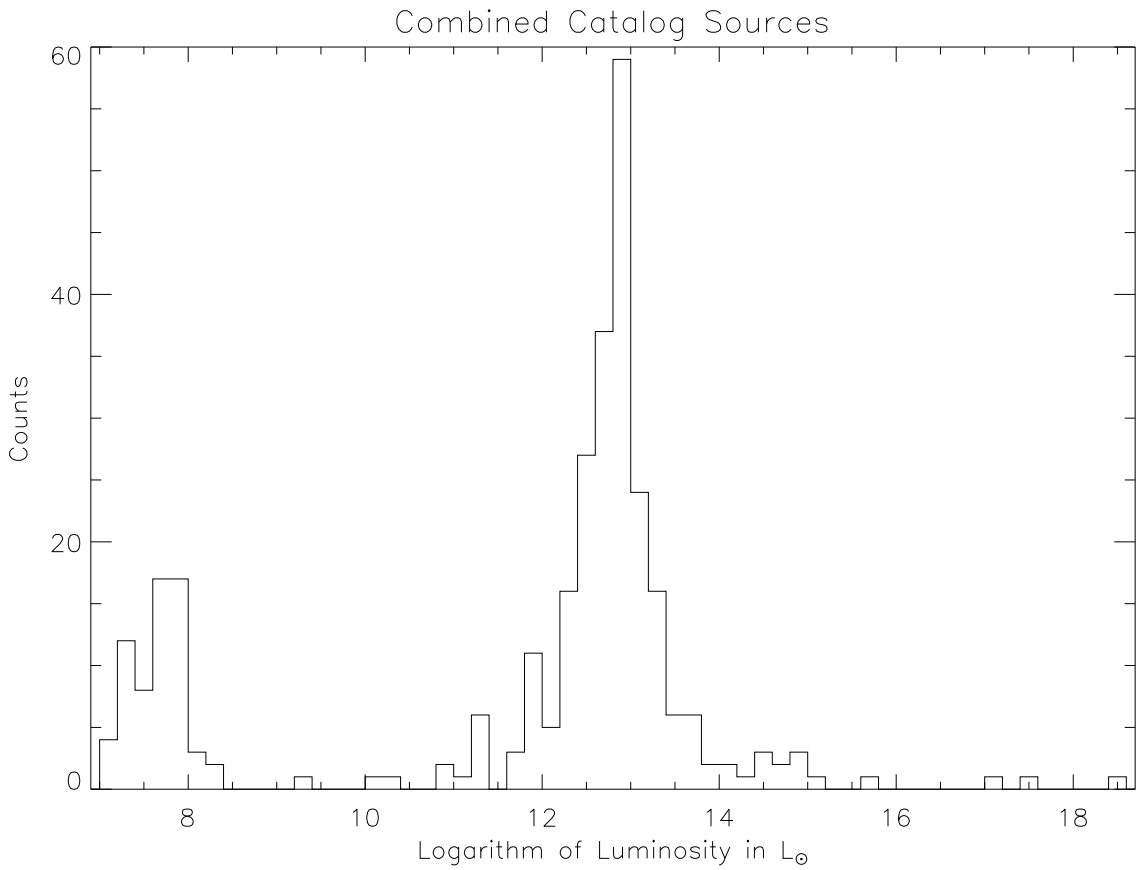

Figure 12: Luminosity histogram of the combined source list. Bin size is 0.2.

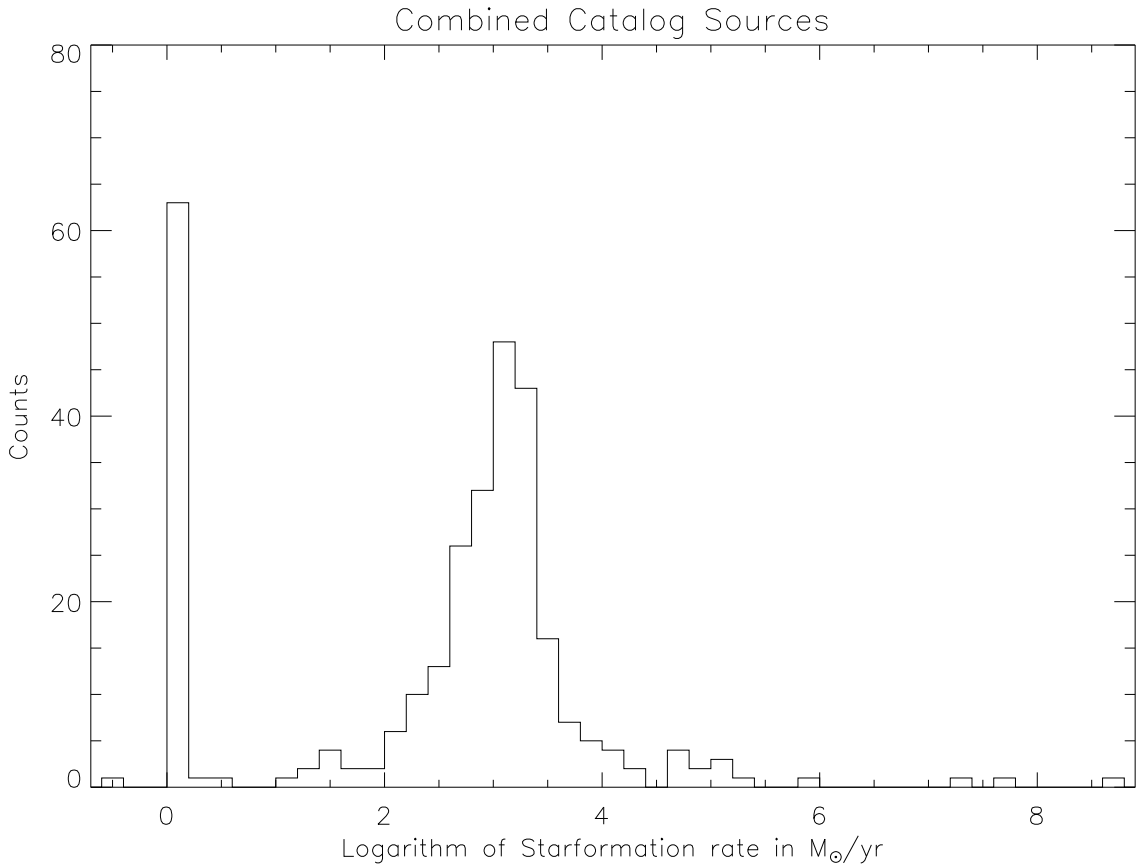

Figure 13: Star formation rate histogram of the combined source list. Bin size is 0.2.

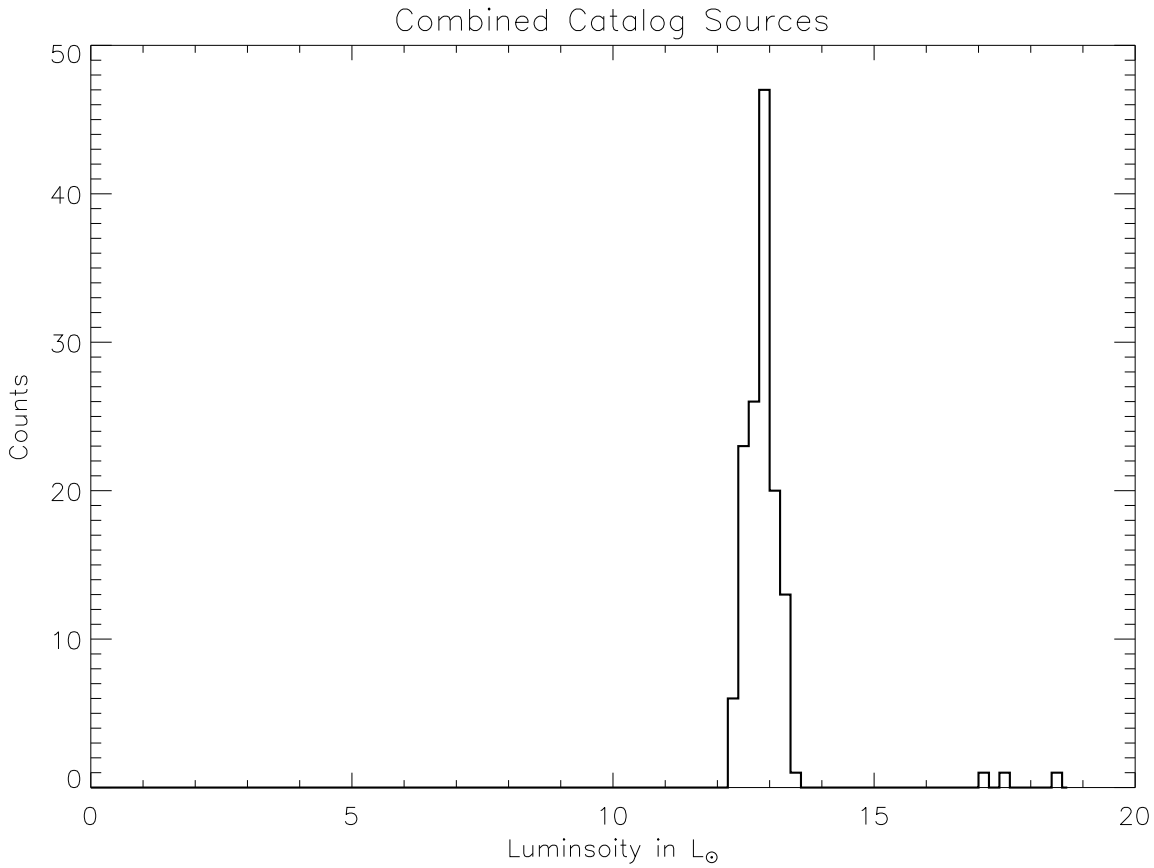

Figure 14: Luminosity of combined source list. Only source with a ratio of luminosity uncertainty over luminosity of less than 10 were counted. The population of low luminosity sources 'disappears'. Note: x axis is in logarithm of luminosity.

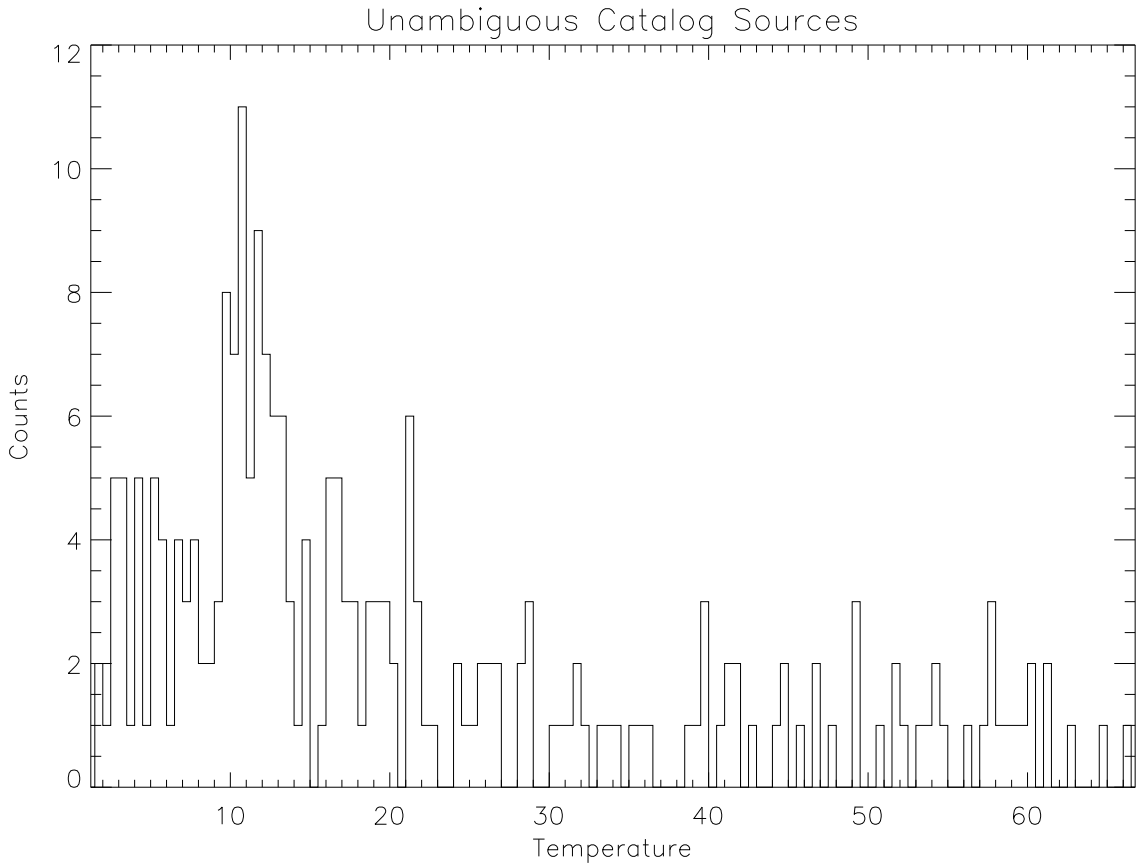

Figure 15: Apparent temperature histogram of the unambiguous source list. Bin size is 0.2.

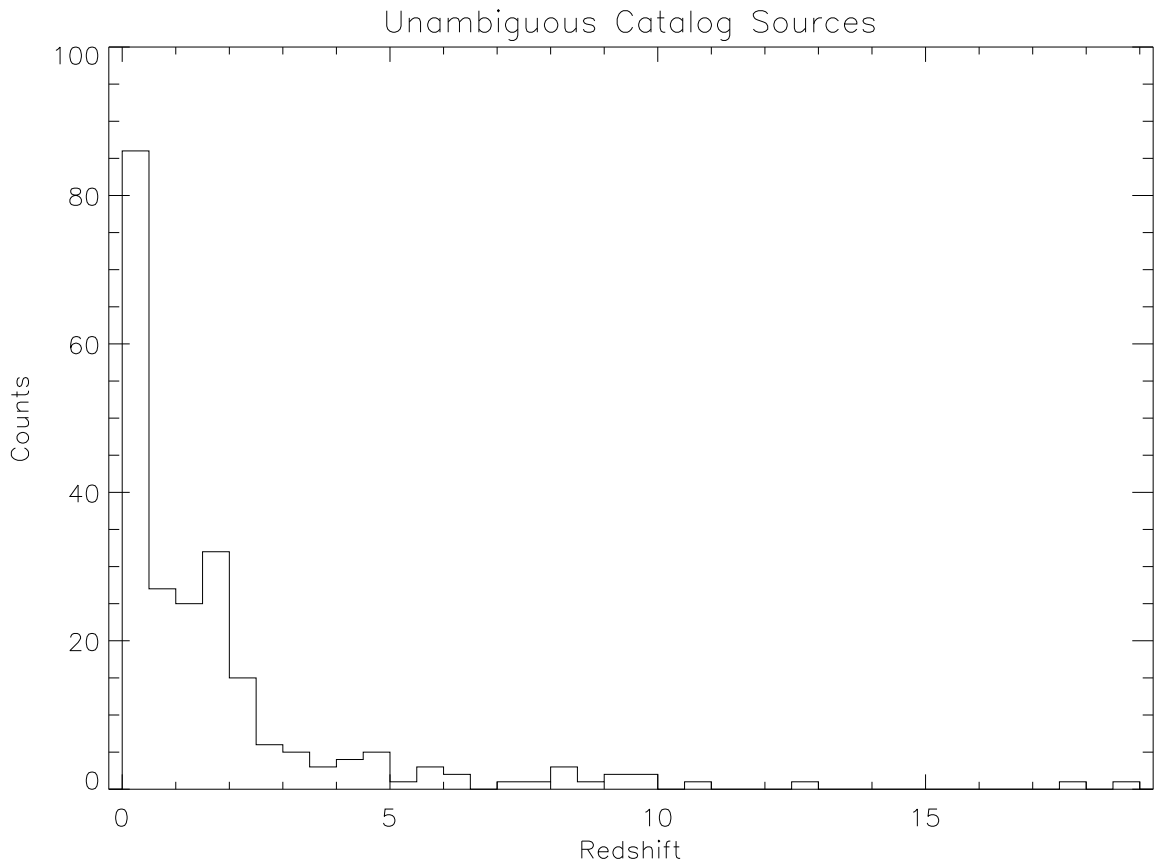

Figure 16: Redshift histogram of the unambiguous source list. Bin size is 0.5.

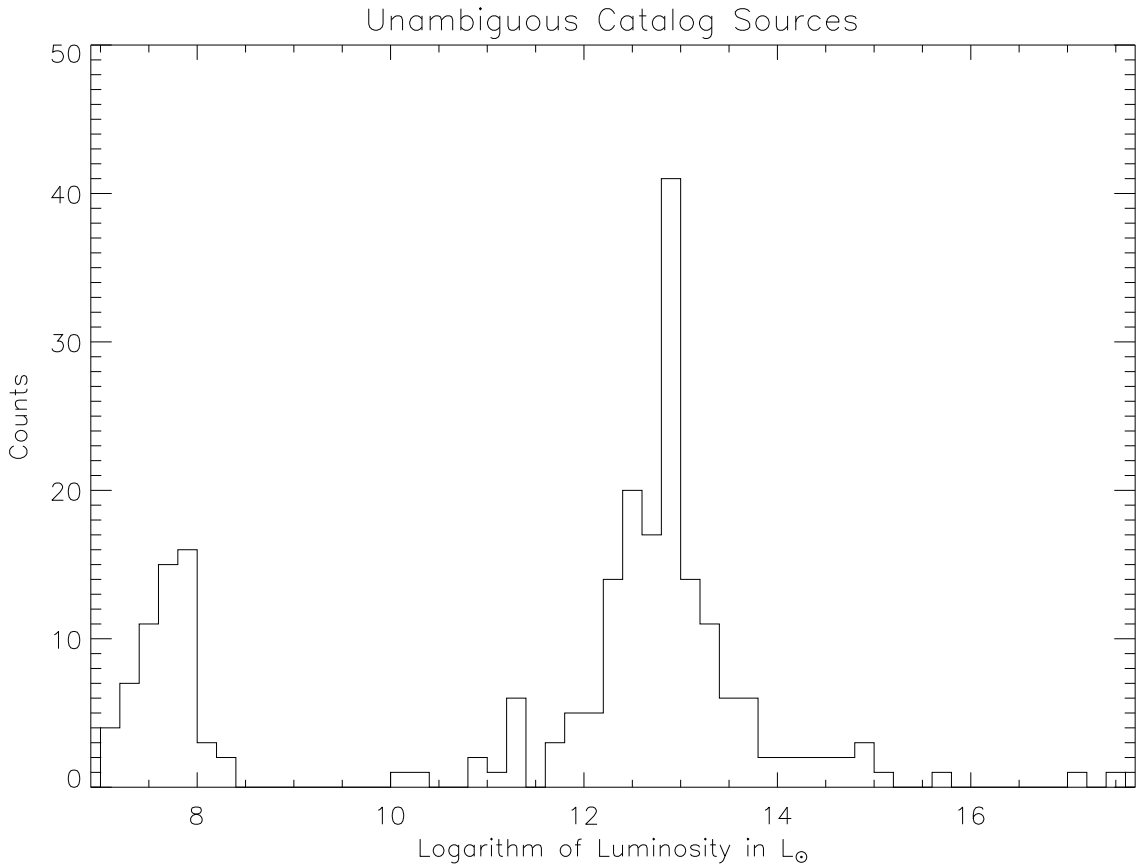

Figure 17: Luminosity histogram of the unambiguous source list. Bin size is 0.2.

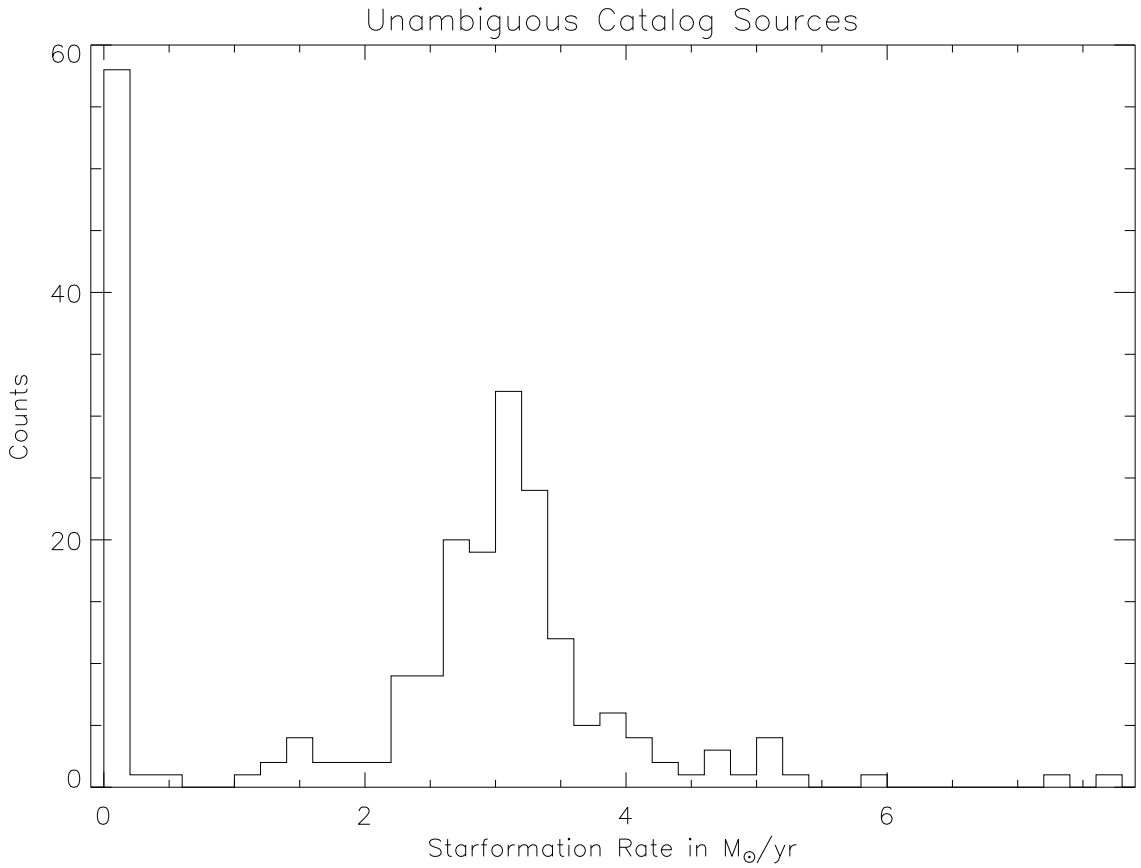

Figure 18: Star formation rate histogram of the unambiguous source list. Bin size is 0.2.

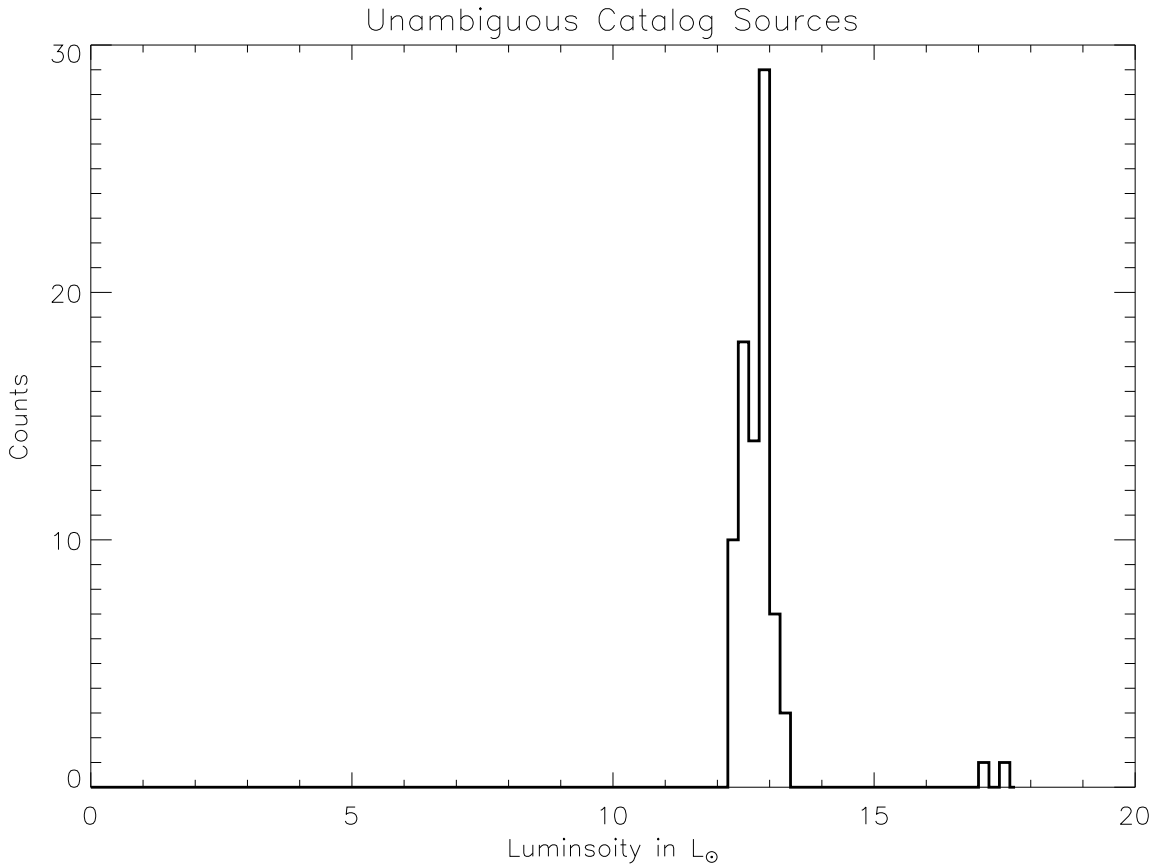

Figure 19: Luminosity of unambiguous source list. Only source with a ratio of luminosity uncertainty over luminosity of less than 10 were counted. The population of low luminosity sources 'disappears'. Note: x axis is in logarithm of luminosity.

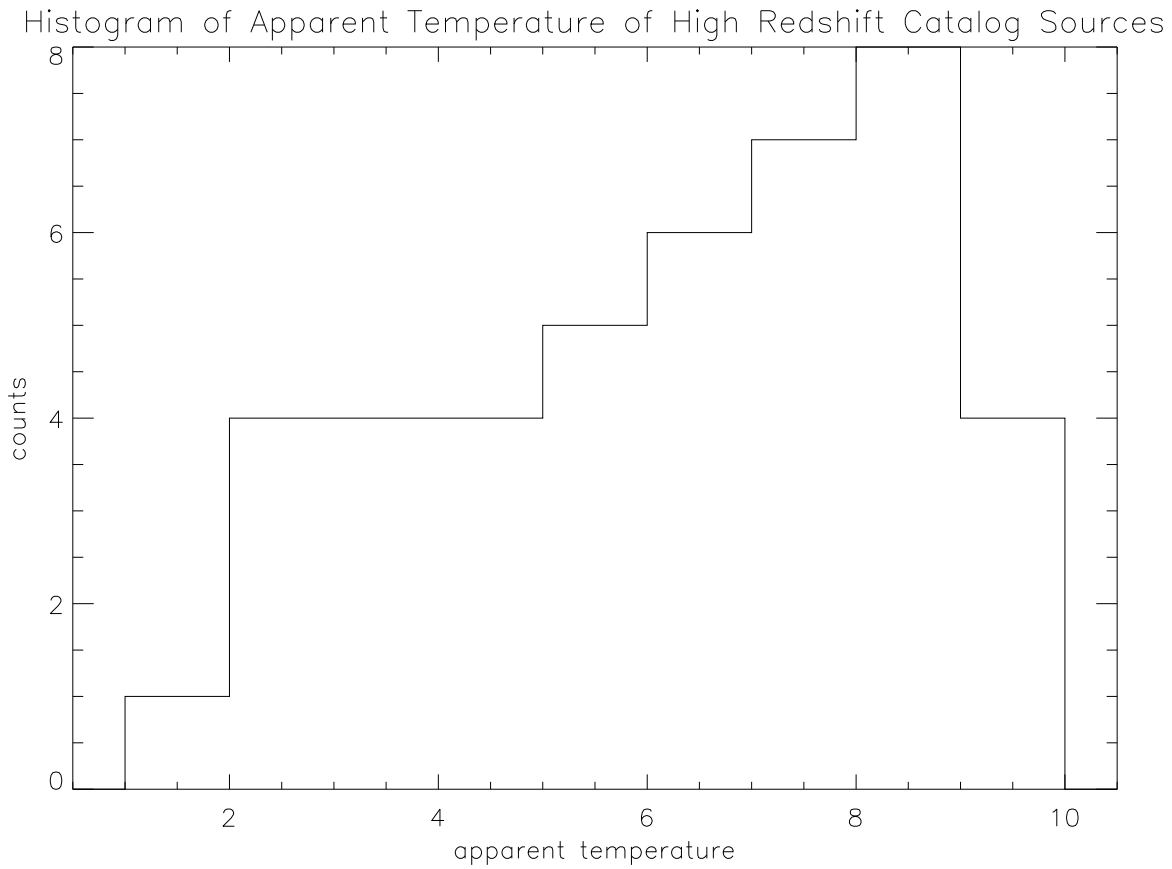

Figure 20: Apparent temperature histogram of the high redshift source list. Bin size is 1.

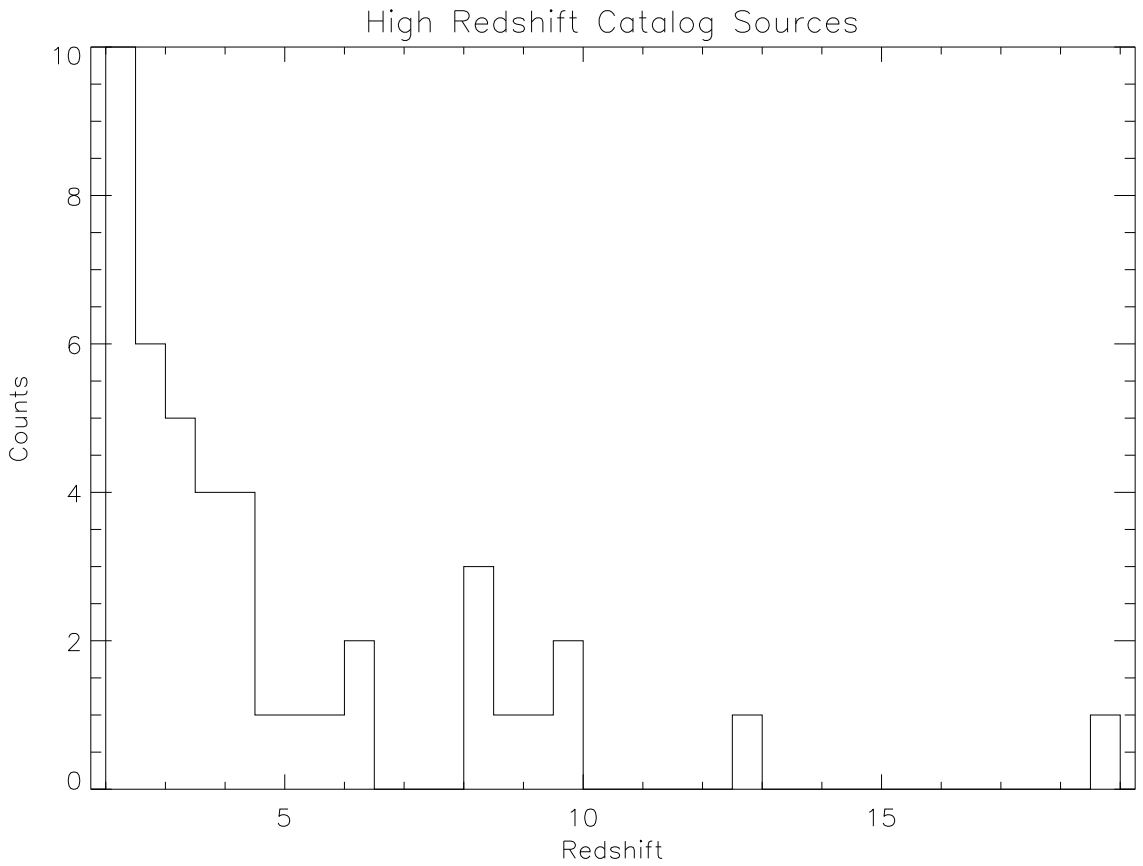

Figure 21: Redshift histogram of the high redshift source list. Bin size is 0.5.

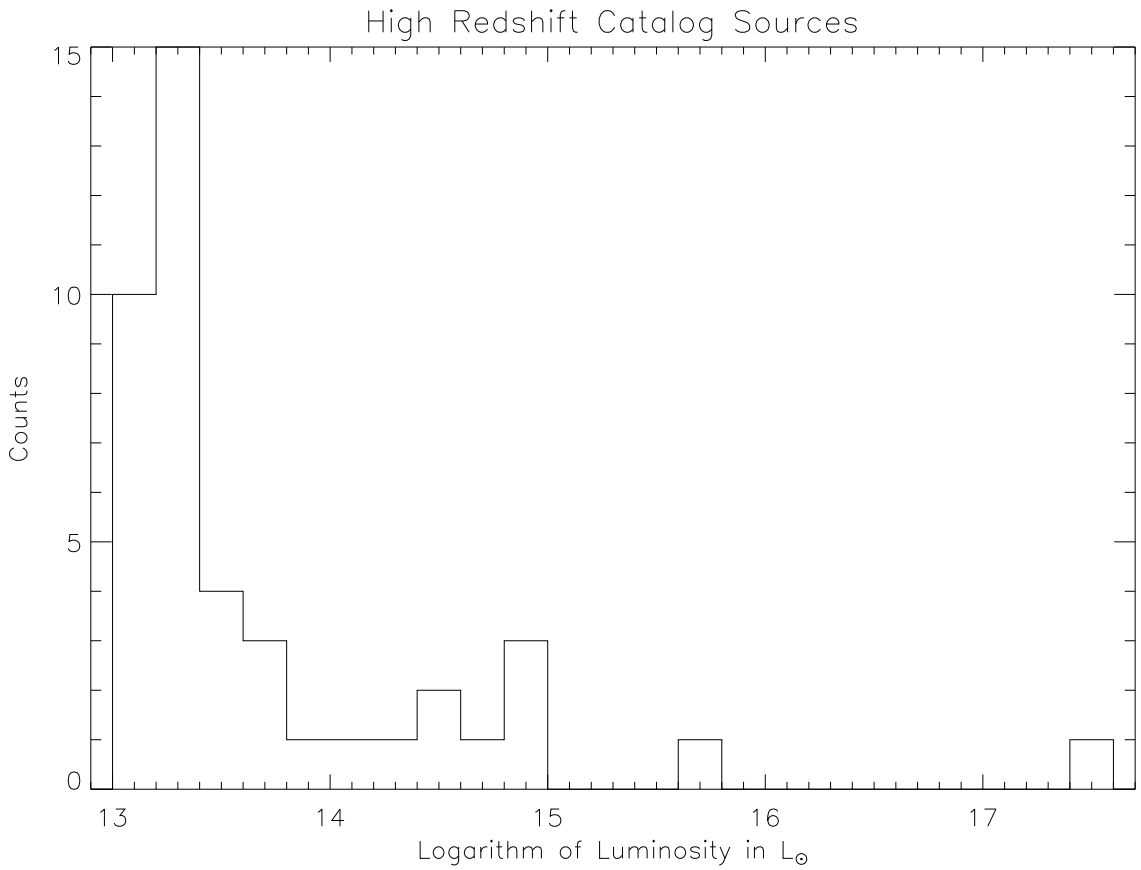

Figure 22: Luminosity histogram of the high redshift source list. Bin size is 0.2.

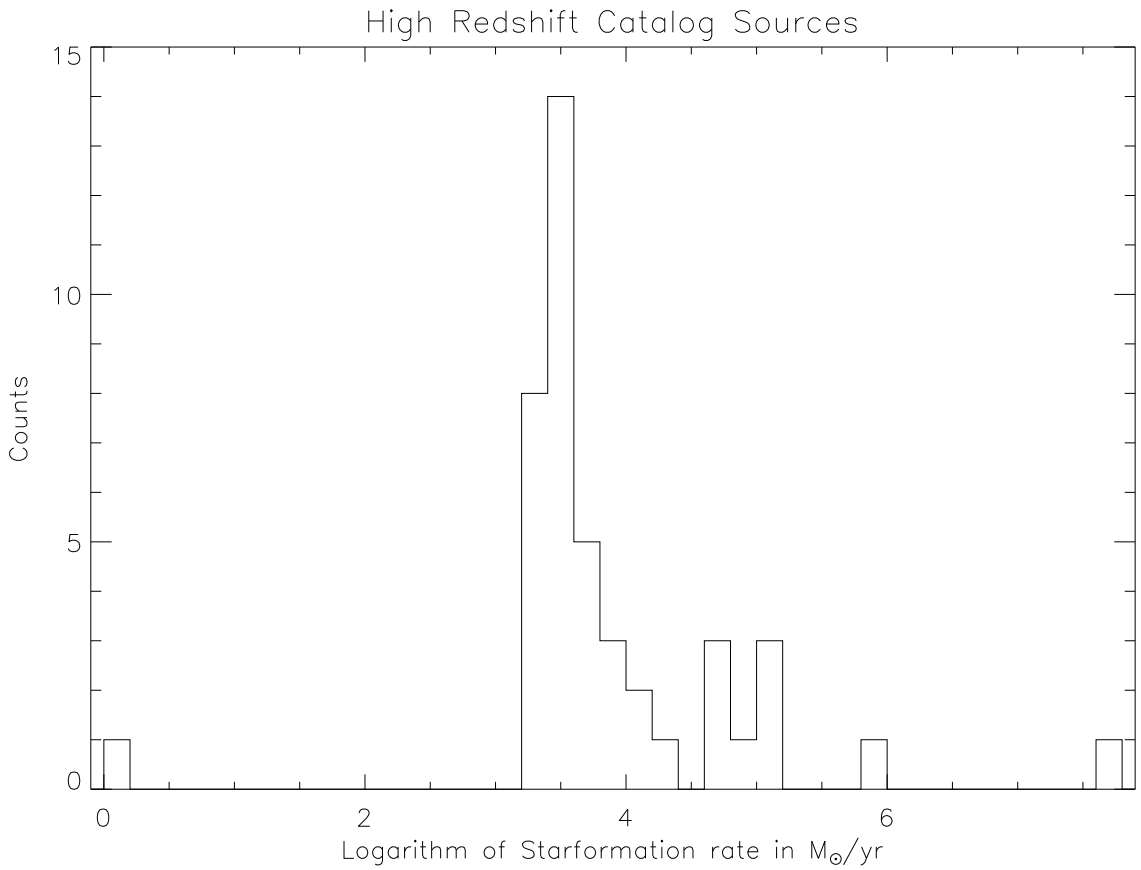

Figure 23: Star formation rate histogram of the high redshift source list. Bin size is 0.2.